Title	Application of the MMG method for the prediction of steady sailing condition and course stability of a ship under external disturbances
Author(s)	Yasukawa, Hironori; Sakuno, Ryoya
Citation	Journal of Marine Science and Technology , 25 : 196 - 220
Issue Date	2020-3
DOI	10.1007/s00773-019-00641-4
Self DOI	
URL	https://ir.lib.hiroshima-u.ac.jp/00050475
Right	This is a post-peer-review, pre-copyedit version of an article published in Journal of Marine Science and Technology. The final authenticated version is available online at: https://doi.org/10.1007/s00773-019-00641-4 This is not the published version. Please cite only the published version. この論文は出版社版ではありません。引用の際には出版社版をご確認、ご利用ください。
Relation	

Application of the MMG-Method for the Prediction of Steady Sailing Condition and Course Stability of a Ship under External Disturbances

Hironori Yasukawa (Hiroshima University)
Ryoya Sakuno (Kawasaki Heavy Industries)

ABSTRACT

For the navigation safety of ships, it is essential to monitor the maneuvering characteristics under external disturbances due to wind and waves. For this purpose, evaluating the average steady sailing conditions such as check helm, speed drop, hull drift angle etc. of a ship moving straight in steady wind and waves is beneficial. In addition, the dynamic stability (course stability) of the ship should be evaluated under its steady sailing condition. This study proposes a method for predicting the steady sailing conditions and course stability under external disturbances, based on the MMG standard method presented by Yasukawa and Yoshimura (2015). The calculation accuracy of the MMG-method has been validated through experiments. The steady sailing conditions and the course stability of a pure car carrier are calculated using the proposed method under external disturbances in deep and shallow waters. In addition, the environmental conditions that limit safe navigation (maneuvering limit) are also discussed, while investigating the effect of the main engine output in particular.

In both deep and shallow waters, a significant effect on the maneuvering limit is observed due to a reduction in engine output. Thus, the presented method is useful in capturing the maneuvering limit of the ship under external disturbances.

Key words

Steady sailing condition; Course stability; Maneuvering limit; MMG-method; Pure car carrier; Adverse weather condition; Main engine output

List of symbols

A_X, A_Y	Front and side profile areas of the ship in air, respectively
A_R	Rudder profile area
a, b	Coefficients of the roll-extinction curve
a_H	Rudder force increase factor
B	Ship breadth
C_b	Block coefficient
C_{XA}, C_{YA}, C_{NA}, C_{KA}	Aerodynamic force coefficients with respect to surge force, lateral force, yaw moment and roll moment, respectively
C_{XW}, C_{YW}, C_{NW}, C_{KW}	Wave-induced steady force coefficients with respect to surge force, lateral force, yaw moment and roll moment in regular waves, respectively
$\overline{C_{XW}}$, $\overline{C_{YW}}$, $\overline{C_{NW}}$, $\overline{C_{KW}}$	Average wave-induced steady force coefficients with respect to surge force, lateral force, yaw moment and roll moment in irregular waves, respectively
D_P	Propeller diameter
d	Ship draft
F_N	Rudder normal force
F_n	Froude number based on ship length
f_A	Correction coefficient when ship heels
f_α	Rudder normal force gradient coefficient
$\overline{GM}$	Metacentric height
$G(\theta)$	Wave direction distribution function
G_1, G_2	Control gains for autopilot
g	Gravity acceleration
$H_{1/3}$	Significant wave height
H_R	Rudder span length
h	Water depth
I_{xx}, I_{zz}	Moment of inertia of the ship around $x-$ and $z-$axes, respectively
J_P	Propeller advance ratio
J_{P0}	Propeller advance ratio during forward motion
J_{xx}, J_{zz}	Added moment of inertia around $x-$ and $z-$axes, respectively
$\overline{KM}$	Metacenter height above baseline
K_T	Propeller thrust open water characteristic
K_Q	Propeller torque open water characteristic
$K_{\dot{\phi}}$, $K_{\dot{\phi}\dot{\phi}}$	Roll damping coefficients
k_{xx}	Radius of roll gyration including added moment of inertia with respect to the roll
k_2, k_1, k_0	Coefficients that represent K_T
L	Ship length between perpendiculars
l_P	Longitudinal coordinate of the propeller position in the formula for β_P
l_R	Effective longitudinal coordinate of the rudder position in the formula for β_R
m	Ship's mass
m_x, m_y	Added masses of the x-axis direction and y-axis direction, respectively

N_{MCR}	Propeller revolution at Maximum Continuous Rating (MCR)
N_{NOR}	Propeller revolution at Normal Rating (NOR)
N'_v, N'_r, N'_ϕ, N'_{vvv} etc.	Hydrodynamic derivatives with respect to yaw moment
n_P	Propeller revolution
$O - x_0y_0z_0$	Space fixed coordinate system
$o - xyz$	Horizontal body fixed coordinate system considering the origin at midship
P_E	Effective power
P_{MCR}	Engine power at MCR
P_{NOR}	Engine power at NOR
Q	Propeller torque
Q_{EMAX}	Maximum propeller torque of the main engines
q_2, q_1, q_0	Coefficients that represent K_Q
R_0	Ship resistance in straight moving
r	Yaw rate
$S_{\zeta\zeta}$	Wave spectrum
T	Propeller thrust
T_P	Average wave period
t	Time
t_P	Thrust deduction fraction
t_R	Steering resistance deduction factor
U	Resultant speed ($= \sqrt{u^2 + v_m^2}$)
U_0	Approach ship speed
U_R	Resultant inflow velocity to the rudder
U_W	Absolute wind velocity
u, v	Surge velocity and lateral velocity at the center of gravity, respectively
u_0, v_0, ψ_0, ϕ_0, δ_0	Steady components of surge velocity, lateral velocity, heading angle, heel angle and rudder angle, respectively
u_A, v_A	Relative surge velocity and lateral velocity component due to wind, respectively
u_R, v_R	Longitudinal and lateral inflow velocity components of the rudder, respectively
V_A	Relative wind velocity
V_S	Design speed of the ship
v_m	Lateral velocity at midship
w_P	Effective wake fraction at the propeller position in maneuvering motions
w_{P0}	Effective wake fraction at the propeller position during forward motion
X, Y, N_m, K_0	Surge force, lateral force, yaw moment, and roll moment with the exception of added mass components, respectively
X_A, Y_A, N_A, K_A	Surge force, lateral force, yaw moment, and roll moment due to wind, respectively
X_H, Y_H, N_H	Surge force, lateral force, and yaw moment acting on the ship hull with the exception of added mass components, respectively
X_P	Surge force due to the propeller

X_R, Y_R, N_R	Surge force, lateral force, and yaw moment by steering, respectively
X_W, Y_W, N_W, K_W	Wave-induced steady surge force, lateral force, yaw moment, and roll moment, respectively
X'_{vv}, X'_{rr}, $X'_{\phi\phi}$, X'_{vr} etc.	Hydrodynamic derivatives with respect to surge force
x_G	Longitudinal coordinate of the center of gravity of the ship
x_H	Longitudinal coordinate of the acting point of the additional lateral force component induced by steering
x_R	Longitudinal coordinate of the rudder position ($=-0.5L$)
Y'_v, Y'_r, Y'_ϕ, Y'_{vvv} etc.	Hydrodynamic derivatives with respect to lateral force
z_G	Vertical coordinate of the center of gravity of the ship
z_H	Vertical coordinate of the acting point of the hull lateral force
z_P	Vertical coordinate of the propeller position
z_R	Vertical coordinate of the acting point of the rudder force
z_W	Vertical coordinate of the acting point of wave-induced lateral force
α_R	Effective inflow angle to the rudder
α_z	Vertical acting point of the lateral added mass component m_y
β	Hull drift angle at midship
β_P	Geometrical inflow angle to the propeller in maneuvering motions
β_R	Effective inflow angle to the rudder in maneuvering motions
γ_R	Flow straightening coefficient
Δu, Δv, $\Delta\psi$, $\Delta\phi$, $\Delta\delta$	Unsteady components of surge velocity, lateral velocity, heading angle, heel angle and rudder angle, respectively
δ	Rudder angle
ϵ	Ratio of the wake fraction at the propeller and rudder positions
η	Ratio of the propeller diameter to the rudder span ($= D_P/H_R$)
η_R	Relative rotative efficiency
θ_A	Relative wind direction
θ_W	Absolute wind direction
κ	Experimental constant for expressing
ρ	Water density
ρ_a	Air density
ϕ	Roll angle
χ	Absolute wave direction
χ_0	Relative wave direction
ψ	Ship heading
∇	Displacement volume of the ship

1 Introduction

Advances in energy conservation in ships have led to opportunities for the evolution of ships with a small main engine. Small engine output generally results in a power margin loss relative to external disturbances, such as wind and waves. Additionally, small engine output leads to a low propeller load thereby reducing the rudder force. Therefore, an excessive reduction in the engine output will result in a potentially unsafe situation wherein a helmsman may not be able to maneuver the ship well in adverse weather conditions. In particular, a pure car carrier (PCC), which has a relatively large superstructure, is significantly influenced by wind. For navigation safety, the maneuvering characteristics of ships in wind and waves need to be captured, and several investigations were conducted for PCCs [1][2][3]. For this purpose, it is useful to evaluate the average steady sailing conditions (SSC), such as check helm, speed drop, hull drift angle, etc., of a ship moving straight in steady wind and waves. In addition, the dynamic stability, or course stability (CS), of the ship should be checked at the SSC. The SSC and the CS of ships under external disturbances are important for discussing the maneuvering limit in adverse weather conditions.

Recently, based on the assumption that the high frequency wave-induced motions are neglected, it has become possible to obtain the SSC by taking the steady sailing characteristics from the maneuvering simulation results in the time domain [2][3][4][5]. However, systematically changing the strength and direction of wind and waves in time domain simulations is complicated. In addition, it is very difficult to evaluate the course stability in adverse weather conditions using the time-domain simulation. Thus, the time-domain based simulation method is inconvenient for obtaining the SSC and the CS under external disturbances.

On the other hand, the basic principle to conveniently obtain the SSC and the CS of the ship in steady wind and waves has already been proposed as follows[6][7]:

1. By setting acceleration, angular acceleration, and angular velocity to zero in the motion equations, the equilibria equations, that is, the balance with respect to forces and moments acting on the ship can be obtained. The SSCs, such as the check helm, speed drop, hull drift angle, and so on are obtained by solving the equilibria equations after setting the environmental condition.

2. The course stability of the ship under adverse conditions is adjudged by evaluating the eigenvalues of the linearized motion equations.

According to the aforementioned ideas, many studies have been performed on the SSC and the CS of ships under external disturbances. However, a remarkable difference can be observed in the existing studies.

The difference exists in the base model of the hydrodynamic forces acting on the maneuvering ship, which can be classified as follows:

- Original MMG-model[8]

- Models expressing the hydrodynamic forces acting on the ship by the polynomial function with respect to ship motions and operation parameters such as rudder angle and propeller revolution (perturbation method)[6][7]

- Simplified model based on the models mentioned above [9][10][11]

The calculation accuracy of the SSC and the CS depends on the accuracy of the base model. Therefore, the base model must be updated based on its progress to ensure reliability. For instance, it is known that the heel or roll effect on the maneuverability cannot be neglected for fine ships, such as container ships and PCCs [13][14][15][16]. However, the heel/roll effects have not been considered in calculations of the SSC and the CS under external disturbances, even though the studied ship is a fine ship. In recent years, a simulation model has been presented by Yasukawa et al. (2019) [17] in consideration of the effect of roll or heel. By using the model, analysis of the SSC and the CS for fine ships becomes possible accurately.

In addition, the following points must be considered. There are two methods to solve the equilibria equations: one is an exact method [12][18][19][20][21][22][23], and the other is an approximate method. For solving the equilibria equations precisely, an iterative calculation is required, with the usage of a computer, since the equilibria equations are mathematically non-linear. In order to obtain the solution in a short time, it is useful to employ approximation partially, although the calculation accuracy becomes worse. In particular, the approximation that the ship speed is known has been often employed in several studies[10][24][25].

Spyrou[19] presented a method to investigate the course stability of ships in steady wind by locally linearized stability analysis at the equilibria condition based on the Jacobean matrix expression that is obtained from the motion equations. This is a general method for solving the problem numerically regardless of the expression of the base hydrodynamic force model. Umeda et al.[23] applied this method for investigating the maneuvering limit of a full hull ship in wind and waves based on the low speed hydrodynamic force model presented by Yoshimura et al.[26][27]. However, the validation of the base model may be insufficient.

In this study, a method is proposed for conveniently obtaining SSC and CS under external disturbances whose special features are as follows:

- Employing 'MMG standard method' [28] as the base model.
- Adding the motion equation of roll [17].
- Considering both wind forces and wave-induced steady forces as external disturbances [5].
- Solving the equilibria equations precisely without approximation.
- Linearizing the motion equations analytically for course stability analysis.

The MMG standard method, which is the base model in the proposed method, has already been validated [28][17]. Additionally, the robustness of course stability analysis is ensured by an analytical treatment in linearizing the base equations. By the proposed method, the SSC and the CS of a PCC under external disturbances are calculated for deep and shallow waters and the limiting environmental conditions for safe navigation (maneuvering limit) are discussed. In particular, the effect of the main engine output is investigated. Previously, there have been no studies on the effect of the main engine output on the SSC and the CS, and the maneuvering limit of the PCC under external disturbances. To conclude the study, the usefulness of the present method in capturing the maneuvering limit of the ship under adverse weather conditions was verified.

2 MMG-based Maneuvering Simulation Method

2.1 Coordinate systems

Fig.1 shows the coordinate systems used in this study. Consider the space fixed coordinate system $O-x_0y_0z_0$, where the x_0-y_0 plane coincides with the still water surface and the z_0-axis is vertically downwards. In addition, consider the horizontal body fixed coordinate system[29] $o-xyz$. The x-axis is taken as the ship's bow direction, the y-axis is the lateral direction and the z-axis is considered vertically downwards. The $x-y$ plane also coincides with the still water surface. Therefore, the origin o is located at the position of the midship on the still water surface.

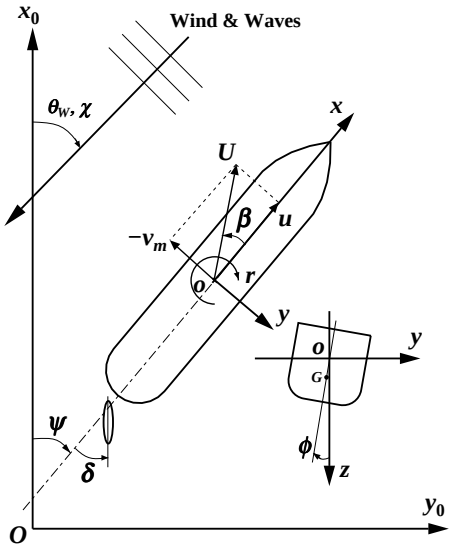

Fig. 1: Coordinate systems

Heading angle ψ is defined as the direction between the x_0-axis and x-axis, and roll angle is denoted by ϕ. Clockwise rotation is positive for roll when observed from the ship's stern to the fore direction. u and v denote the velocity components of the x-axis and y-axis directions respectively, and r is the yaw rate around the z-axis. δ denotes the rudder angle. The center of gravity G is approximately located at the position (x_G, 0, z_G). Among z_G, for the metacentric height $\overline{GM}$ and the metacenter height from the ship's bottom $\overline{KM}$, the following relation holds:

$$z_G \simeq \overline{GM} - \overline{KM} + d \tag{1}$$

where d is ship draft. Then, the lateral velocity component at midship position v_m is expressed using the velocity component at the center of gravity as:

$$v_m = v - x_G r + z_G \dot{\phi} \tag{2}$$

The hull drift angle at midship position β is evaluated by

$$\beta = \tan^{-1}(-v_m/u) \tag{3}$$

and total velocity U is defined as:

$$U = \sqrt{u^2 + v_m^2} \tag{4}$$

The main wave propagation direction is denoted as χ as shown in Fig.1. Then, the relative wave direction χ_0 is defined as $\chi_0 \equiv \chi - \psi$. The head wave of the ship is defined as $\chi_0 = 0°$, the beam wave as $\chi_0 = 90°$, and the following wave as $\chi_0 = 180°$. The wind direction θ_W is assumed to be the same as the wave direction χ.

2.2 Motion equations

In the horizontal body fixed coordinate system, the motion equations for surge, sway, yaw, and roll of a ship are expressed as[17]:

$$\left.\begin{aligned}
(m+m_x)\dot{u} - (m+m_y)v_m r - mx_G r^2 + mz_G r\dot{\phi} &= X \\
(m+m_y)\dot{v}_m + (m+m_x)ur + mx_G\dot{r} - (m_y\alpha_z + mz_G)\ddot{\phi} &= Y \\
(I_{zz} + J_{zz} + mx_G^2)\dot{r} + mx_G(\dot{v}_m - z_G\ddot{\phi} + ur) &= N \\
(I_{xx} + J_{xx} + mz_G^2)\ddot{\phi} - (m_y\alpha_z + mz_G)\dot{v}_m - mz_G(x_G\dot{r} + ur) &= K
\end{aligned}\right\} \tag{5}$$

Here, m is the ship's mass, and I_{xx} and I_{zz} are the moment of inertias for roll and yaw, respectively. m_x, m_y, J_{zz} and J_{xx} denote added mass for surge, added mass for sway, added moment of inertia for yaw, and added moment of inertia for roll, respectively. α_z is the vertical acting point of the lateral added mass component m_y. X is the surge force excluding added mass component, Y is the lateral force excluding added mass component, N is the yaw moment around midship excluding added moment of inertia component, and K is the roll moment around x-axis excluding added moment of inertia component. In the equations, the dot notation means ordinary differential with respect to time t. The unknown variables in the motion equations are longitudinal velocity component u, lateral velocity component v_m, yaw rate r, and roll angle ϕ. These motion equations are the base equations to be solved.

X, Y and N are expressed as:

$$\left.\begin{aligned}
X &= X_H + X_R + X_P + X_A + X_W \\
Y &= Y_H + Y_R + Y_A + Y_W \\
N &= N_H + N_R + N_A + N_W
\end{aligned}\right\} \tag{6}$$

Subscripts H, R and P on the right hand side of Eq.(6) denote hull, rudder, and propeller, respectively. Subscripts A and W are aerodynamic force and wave-induced steady force (wave drift forces), respectively.

Roll moment K is expressed as[17]:

$$K = -Y_H z_H - Y_R z_R - mg\overline{GM}\phi + K_{\dot{\phi}}\dot{\phi} + K_{\dot{\phi}\dot{\phi}}\dot{\phi}|\dot{\phi}| + K_A + K_W \tag{7}$$

In the right hand side of Eq.(7), the first term is the roll moment acting on the hull except roll restoring moment, and the 2nd term is the roll moment due to steering, and they are expressed by multiplying the lateral force components (Y_H, Y_R) to their vertical acting points (z_H, z_R). The 3rd term is roll restoring moment, and the 4th and the 5th terms are

roll damping moments. $K_{\dot{\phi}}$ and $K_{\dot{\phi}\dot{\phi}}$ which are the roll damping coefficients, are expressed as follows:

$$K_{\dot{\phi}} = -\frac{2}{\pi} a \sqrt{mg\overline{GM}(I_{xx} + J_{xx})} \tag{8}$$

$$K_{\dot{\phi}\dot{\phi}} = -0.75b \left(\frac{180}{\pi}\right) (I_{xx} + J_{xx}) \tag{9}$$

where a and b are the coefficients of roll-extinction curve obtained by a roll decay test.

2.3 Hull hydrodynamic forces

Hydrodynamic forces acting on ship hull (X_H, Y_H, N_H) are expressed as:

$$\left.\begin{aligned} X_H &= (1/2)\rho L d U^2 \; X'_H(v'_m, r', \phi) \\ Y_H &= (1/2)\rho L d U^2 \; Y'_H(v'_m, r', \phi) \\ N_H &= (1/2)\rho L^2 d U^2 \; N'_H(v'_m, r', \phi) \end{aligned}\right\} \tag{10}$$

Here, X'_H, Y'_H and N'_H are expressed as:

$$\begin{aligned} X'_H(v'_m, r', \phi) &= -R'_0 + X'_{vv} v'^2_m + X'_{vr} v'_m r' + X'_{rr} r'^2 + X'_{vvvv} v'^4_m + X'_{v\phi} v'_m \phi \\ &\quad + X_{r\phi} r' \phi + X'_{\phi\phi} \phi^2 \end{aligned} \tag{11}$$

$$\begin{aligned} Y'_H(v'_m, r', \phi) &= Y'_v v'_m + Y'_r r' + Y'_{vvv} v'^3_m + Y'_{vvr} v'^2_m r' + Y'_{vrr} v'_m r'^2 + Y'_{rrr} r'^3 \\ &\quad + Y'_\phi \phi + Y'_{vv\phi} v'^2_m \phi + Y'_{v\phi\phi} v'_m \phi^2 + Y'_{rr\phi} r'^2 \phi + Y'_{r\phi\phi} r' \phi^2 \end{aligned} \tag{12}$$

$$\begin{aligned} N'_H(v'_m, r', \phi) &= N'_v v'_m + N'_r r' + N'_{vvv} v'^3_m + N'_{vvr} v'^2_m r' + N'_{vrr} v'_m r'^2 + N'_{rrr} r'^3 \\ &\quad + N'_\phi \phi + N'_{vv\phi} v'^2_m \phi + N'_{v\phi\phi} v'_m \phi^2 + N'_{rr\phi} r'^2 \phi + N'_{r\phi\phi} r' \phi^2 \end{aligned} \tag{13}$$

Here, R'_0 is the resistance coefficient in straight motion, and X'_{vv}, Y'_v, N'_v etc. are called the hydrodynamic derivatives on maneuvering. X'_H is expressed as the sum of R'_0, and the 2nd order polynomial function of v'_m, r' and ϕ except for X'_{vvvv}-term, and Y'_H and N'_H are expressed as the 1st and 3rd order polynomial functions of v'_m, r' and ϕ[15].

2.4 Propeller force

Propeller force (X_P) is expressed as:

$$X_P = (1 - t_P)T \tag{14}$$

where t_P is thrust deduction fraction. Then, propeller thrust T and torque Q are expressed as:

$$T = \rho n_P^2 D_P^4 \; K_T(J_P) \tag{15}$$

$$Q = \rho n_P^2 D_P^5 \; K_Q(J_P)/\eta_R \tag{16}$$

where n_P is propeller revolution, D_P is propeller diameter and η_R is relative rotative efficiency. The propeller thrust open water characteristic K_T and the torque open water characteristic K_Q are expressed as:

$$K_T(J_P) = k_2 J_P^2 + k_1 J_P + k_0 \tag{17}$$

$$K_Q(J_P) = q_2 J_P^2 + q_1 J_P + q_0 \tag{18}$$

where k_2, k_1 and k_0 are coefficients representing K_T, and q_2, q_1 and q_0 are coefficients representing K_Q. J_P is propeller advance ratio and expressed as:

$$J_P = \frac{u(1-w_P)}{n_P D_P} \tag{19}$$

where w_P is wake fraction at the propeller position, and is expressed as a function of the geometrical inflow angle to the propeller β_P as[30]:

$$w_P = w_{P0}\left[1-\left(1-\cos^2\beta_P\right)\left(1-|\beta_P|\right)\right] \tag{20}$$

Here β_P is defined as $\beta_P \equiv \beta - l'_P r' + z'_P \dot{\phi}'$ where l'_P and z'_P are non-dimensional longitudinal and vertical coordinates of the propeller position, respectively. w_{P0} is wake fraction at the propeller position in straight motion.

2.5 Rudder forces

Effective rudder forces (X_R, Y_R, N_R) are expressed as[17]:

$$\left.\begin{aligned} X_R &= -(1-t_R)F_N \sin\delta\cos\phi \\ Y_R &= -(1+a_H)F_N\cos\delta\cos\phi \\ N_R &= -(x_R+a_H x_H)F_N\cos\delta\cos\phi \end{aligned}\right\} \tag{21}$$

where δ is the rudder angle, F_N is the rudder normal force, and t_R, a_H and x_H are coefficients representing the hydrodynamic interaction between ship hull and rudder. As shown on the right-hand side of Eq.(21), $\cos\phi$ is multiplied to F_N to consider the roll effect. F_N is expressed as:

$$F_N = (1/2)\rho A_R U_R^2 f_\alpha \sin\alpha_R \tag{22}$$

where A_R is the rudder area and f_α is the rudder lift gradient coefficient. The resultant inflow velocity to rudder U_R and effective inflow angle to rudder α_R are expressed as:

$$U_R = \sqrt{u_R^2+v_R^2} \tag{23}$$

$$\alpha_R = \delta - \tan^{-1}(v_R/u_R) \tag{24}$$

u_R and v_R are longitudinal and lateral inflow velocity components to the rudder, respectively. v_R is expressed as [28]:

$$v_R = U\ \gamma_R\ \beta_R \tag{25}$$

where γ_R is the flow straightening coefficient, and β_R is the geometrical inflow angle to the rudder, and defined as $\beta_R \equiv \beta - l'_R r' + z'_R \dot{\phi}'$. u_R is expressed as[2][31]:

$$u_R = \epsilon\, u(1-w_{P0})\sqrt{\eta\left\{1+\kappa\left(\sqrt{1+\frac{8K_T(J_{P0})}{\pi J_{P0}^2}}-1\right)\right\}^2+(1-\eta)} \tag{26}$$

where ϵ denotes the ratio of wake coefficient at the propeller and rudder positions, κ is an experimental constant for expressing u_R, and η is the ratio of propeller diameter to rudder span ($= D_P/H_R$ where H_R denotes the rudder span length). J_{P0} denotes the propeller advance ratio in moving straight.

2.6 Wind forces

As the external forces due to wind, the forces and the moments in the constant and unifrom wind are considered. They (X_A, Y_A, N_A, K_A) are expressed as:

$$\left.\begin{aligned} X_A &= (1/2)\rho_a A_X V_A^2 C_{XA}(\theta_A) \\ Y_A &= (1/2)\rho_a A_Y V_A^2 C_{YA}(\theta_A) f_A(\phi) \\ N_A &= (1/2)\rho_a A_Y V_A^2 L\, C_{NA}(\theta_A) f_A(\phi) \\ K_A &= (1/2)\rho_a A_Y V_A^2 L\, C_{KA}(\theta_A) f_A(\phi) \end{aligned}\right\} \tag{27}$$

where

$$\theta_A = \tan^{-1}(v_A/u_A) \tag{28}$$
$$V_A^2 = u_A^2 + v_A^2 \tag{29}$$
$$u_A = u + U_W \cos(\theta_W - \psi) \tag{30}$$
$$v_A = v + U_W \sin(\theta_W - \psi) \tag{31}$$

Here, ρ_a denotes the air density. A_X and A_Y are front and side profile areas of the ship in contact with air, respectively. V_A denotes the relative wind velocity, U_W the absolute wind velocity, θ_A the relative wind direction, and θ_W the absolute wind direction. $\theta_A = 0°$ is the head wind for the ship, $\theta_A = 180°$ is the following wind and $\theta_A = 90°$ is the lateral wind. C_{XA}, C_{YA}, C_{NA} and C_{KA} denote the aerodynamic force coefficients, which are expressed as a function of θ_A. $f_A(\phi)$ is the correction coefficient when ship heels and is expressed as $f_A = -0.355\phi + 1$[21].

2.7 Wave-induced steady forces

As the external forces due to waves, the average values of the wave-induced steady forces (added resistance, steady lateral force, steady yaw moment, and steady roll moment) in irregular waves are used. These are calculated using the short-term prediction technique based on the wave-induced steady force coefficients in regular waves. Then, the average values of the wave-induced steady forces in irregular waves (X_W, Y_W, N_W, K_W) are expressed as:

$$\left.\begin{aligned} X_W &= \rho g H_{1/3}^2 L\, \overline{C_{XW}}(U, T_P, \chi_0) \\ Y_W &= \rho g H_{1/3}^2 L\, \overline{C_{YW}}(T_P, \chi_0) \\ N_W &= \rho g H_{1/3}^2 L^2\, \overline{C_{NW}}(T_P, \chi_0) \\ K_W &= -Y_W z_W \end{aligned}\right\} \tag{32}$$

where $H_{1/3}$ is the significant wave height and g is the gravitational acceleration. $\overline{C_{XW}}$, $\overline{C_{YW}}$ and $\overline{C_{NW}}$ are the wave-induced steady force coefficients in irregular waves. It is assumed that $\overline{C_{YW}}$ and $\overline{C_{NW}}$ bear no relation to ship speed U, although $\overline{C_{XW}}$ is the function of U with the average wave period T_P and relative wave direction χ_0. As $\overline{C_{YW}}$ and $\overline{C_{NW}}$, those values without forward speed ($U = 0$) are used in the calculations [32].

$\overline{C_{XW}}$, $\overline{C_{YW}}$ and $\overline{C_{NW}}$ are expressed as:

$$\left.\begin{aligned}
\overline{C_{XW}}(U,T_P,\chi_0) &= 2\int_{-\pi}^{\pi} G(\theta)d\theta \int_0^{\infty} C_{XW}(U,\omega,\chi_0)\frac{S_{\zeta\zeta}(\omega)}{H_{1/3}^2}d\omega \\
\overline{C_{YW}}(T_P,\chi_0) &= 2\int_{-\pi}^{\pi} G(\theta)d\theta \int_0^{\infty} C_{YW}(\omega,\chi_0)\frac{S_{\zeta\zeta}(\omega)}{H_{1/3}^2}d\omega \\
\overline{C_{NW}}(T_P,\chi_0) &= 2\int_{-\pi}^{\pi} G(\theta)d\theta \int_0^{\infty} C_{NW}(\omega,\chi_0)\frac{S_{\zeta\zeta}(\omega)}{H_{1/3}^2}d\omega
\end{aligned}\right\} \tag{33}$$

Here, C_{XW}, C_{YW} and C_{NW} are the wave-induced steady force coefficients in regular waves. $S_{\zeta\zeta}(\omega)$ is the wave spectrum, and $G(\theta)$ is the wave direction distribution function.

3 Base Equations for Obtaining Steady Sailing Condition and Course Stability under External Disturbances

The ship's behavior after a small disturbance acts on it when moving in wind and waves, is considered. Here, the variables in the motion equations, u, v_m, ψ, ϕ and δ, are expressed as the sum of the static (steady term) and variable components (unsteady term):

$$\left.\begin{array}{rcl} u &=& u_0 \\ v_m &=& v_0 + \Delta v \\ \psi &=& \psi_0 + \Delta\psi \\ \phi &=& \phi_0 + \Delta\phi \\ \delta &=& \delta_0 + \Delta\delta \end{array}\right\} \tag{34}$$

In Eq.(34), the subscript 0 implies a steady term, and substituting Δ implies an unsteady term. The steady terms are assumed to be $O(1)$, and the unsteady terms are assumed to be $O(\varepsilon)$ where ε is a small quantity. In addition, it is assumed that ψ_0 is given, and the unsteady term of u (Δu) is not considered, for simplicity. Substituting Eq.(34) to the motion equations Eq.(5), two sets of the motion equations can be obtained for the steady and the unsteady terms. The motion equations for the steady terms are obtained by setting the acceleration, angular acceleration, and angular velocity terms to zero in Eq.(5). The motion equations for the unsteady terms are obtained by eliminating the higher order terms of ε in the equations, namely, linearizing the motion equations. The course stability of the ship can be evaluated based on the linearized motion equations.

3.1 Equilibria equations and its calculation scheme

Equations for the steady terms (equilibria equations) are expressed as follows:

$$\begin{aligned} 0 &= X_H(u_0, v_0, \phi_0) - (1-t_R)F_N(u_0, v_0, \delta_0)\sin\delta_0\cos\phi_0 + (1-t_P)T(u_0, v_0) \\ &\quad + X_A(u_0, v_0, \phi_0, \psi_0) + X_W(u_0, v_0, \psi_0) \qquad (35) \\ 0 &= Y_H(u_0, v_0, \phi_0) - (1+a_H)F_N(u_0, v_0, \delta_0)\cos\delta_0\cos\phi_0 + Y_A(u_0, v_0, \phi_0, \psi_0) \\ &\quad + Y_W(\psi_0) \qquad (36) \\ 0 &= N_H(u_0, v_0, \phi_0) - (x_R + a_H x_H)F_N(u_0, v_0, \delta_0)\cos\delta_0\cos\phi_0 + N_A(u_0, v_0, \phi_0, \psi_0) \\ &\quad + N_W(\psi_0) \qquad (37) \\ 0 &= -Y_H(u_0, v_0, \phi_0)z_H + (1+a_H)F_N(u_0, v_0, \delta_0)\cos\delta_0\cos\phi_0 z_R - mg\overline{GM}\phi_0 \\ &\quad + K_A(u_0, v_0, \phi_0, \psi_0) + K_W(\psi_0) \qquad (38) \end{aligned}$$

Eqs.(35) to (38) represent a balance of hull forces, rudder forces, propeller forces, and external forces due to wind and waves. The unknown variables are u_0, v_0, ϕ_0 and δ_0. The above-mentioned equations are non-linear, and hence a special method is needed to solve the equations efficiently. For this purpose, consider a deformation of the equations. By eliminating $F_N\cos\delta_0\cos\phi_0$ in Eqs.(36) and (37), the following equation is obtained:

$$\begin{aligned} 0 &= (x_R + a_H x_H)\left[Y_H(u_0, v_0, \phi_0) + Y_A(u_0, v_0, \phi_0, \psi_0) + Y_W(\psi_0)\right] \\ &\quad -(1+a_H)\left[N_H(u_0, v_0, \phi_0) + N_A(u_0, v_0, \phi_0, \psi_0) + N_W(\psi_0)\right] \qquad (39) \end{aligned}$$

Similarly, by eliminating $F_N \cos\delta_0 \cos\phi_0$ in Eqs.(36) and (38), the following equation is obtained:

$$\begin{aligned} 0 &= Y_H(u_0, v_0, \phi_0)(z_R - z_H) - mg\overline{GM}\phi_0 + K_A(u_0, v_0, \phi_0, \psi_0) + K_W(\psi_0) \\ &\quad + [Y_A(u_0, v_0, \phi_0, \psi_0) + Y_W(\psi_0)]z_R \end{aligned} \tag{40}$$

Eqs.(39) and (40) are not the function of rudder angle δ_0. These equations are used as the base equations to be solved.

The Regula–Falsi method is used for obtaining the solution of the non-linear equations numerically. The calculation scheme is as follows:

1. Set propeller revolution n_P and external force conditions.
2. Set initial value of u_0 for solving Eq.(35) by the Regula–Falsi method.
3. Obtain v_0 and ϕ_0 by solving Eqs.(39) and (40).
4. Obtain δ_0 by solving Eq.(37).
5. Update u_0 by iteration, until Eq.(35) is satisfied.

3.2 Linearized motion equations and course stability

The linearized motion equations for the unsteady terms are expressed as follows:

$$[A]\{\dot{x}\} = [B]\{x\} + \{d\}\Delta\delta \tag{41}$$

where

$$[A] = \begin{bmatrix} a_1 & a_2 & a_3 & 0 & 0 \\ a_4 & a_5 & a_6 & 0 & 0 \\ a_7 & a_8 & a_9 & 0 & 0 \\ 0 & 0 & 0 & 1 & 0 \\ 0 & 0 & 0 & 0 & 1 \end{bmatrix}, \qquad [B] = \begin{bmatrix} b_1 & b_2 & b_3 & b_4 & b_5 \\ b_6 & b_7 & b_8 & b_9 & b_{10} \\ b_{11} & b_{12} & b_{13} & b_{14} & b_{15} \\ 0 & 1 & 0 & 0 & 0 \\ 0 & 0 & 1 & 0 & 0 \end{bmatrix} \tag{42}$$

$$\{x\} = \begin{Bmatrix} \Delta v \\ \Delta r \\ \Delta\dot{\phi} \\ \Delta\psi \\ \Delta\phi \end{Bmatrix}, \qquad \{d\} = \begin{Bmatrix} d_1 \\ d_2 \\ d_3 \\ 0 \\ 0 \end{Bmatrix} \tag{43}$$

In $[A]$, $[B]$ and $\{d\}$ matrices, a_1 to a_9, b_1 to b_{15} and d_1 to d_3 are expressed as follows:

$$\begin{aligned} a_1 &= m + m_y \\ a_2 &= x_G m \\ a_3 &= -(m_y\alpha_z + mz_G) \\ a_4 &= x_G m \\ a_5 &= I_{zz} + J_{zz} + mx_G^2 \\ a_6 &= -mz_G x_G \\ a_7 &= -(m_y\alpha_z + mz_G) \\ a_8 &= -mz_G x_G \\ a_9 &= I_{xx} + J_{xx} + mz_G^2 \end{aligned}$$

$$
\begin{aligned}
b_1 &= F_{Hv1} + F_{Rv1} + F_{Av1} \\
b_2 &= -(m + m_x)u_0 + F_{Hr1} + F_{Rr1} \\
b_3 &= F_{R\dot{\phi}1} \\
b_4 &= F_{A\psi 1} + F_{W\psi 1} \\
b_5 &= F_{H\phi 1} + F_{R\phi 1} + F_{A\phi 1} \\
b_6 &= F_{Hv2} + F_{Rv2} + F_{Av2} \\
b_7 &= -mx_G u_0 + F_{Hr2} + F_{Rr2} \\
b_8 &= F_{R\dot{\phi}2} \\
b_9 &= F_{A\psi 2} + F_{W\psi 2} \\
b_{10} &= F_{H\phi 2} + F_{R\phi 2} + F_{A\phi 2} \\
b_{11} &= F_{Hv3} + F_{Rv3} + F_{Av3} \\
b_{12} &= mz_G u_0 + F_{Hr3} + F_{Rr3} \\
b_{13} &= K_{\dot{\phi}} + F_{R\dot{\phi}3} \\
b_{14} &= F_{A\psi 3} + F_{W\psi 3} \\
b_{15} &= F_{H\phi 3} + F_{R\phi 3} + F_{A\phi 3} \\
d_1 &= F_{R\delta 1} \\
d_2 &= F_{R\delta 2} \\
d_3 &= F_{R\delta 3}
\end{aligned}
$$

For the 1st subscript of F appearing in the above-mentioned equations, H denotes hull hydrodynamic forces, R denotes rudder forces, A denotes aerodynamic forces, and W denotes wave-induced steady forces. The 2nd subscript of F is the parameter for partial differential, and the 3rd subscript numbers 1, 2, and 3 denote the lateral force, yaw moment, and roll moment, respectively. For instance, $F_{Hvi}(i = 1, 2, 3)$ is expressed as:

$$
\begin{aligned}
F_{Hv1} &\equiv \frac{\partial Y_H}{\partial v} \\
F_{Hv2} &\equiv \frac{\partial N_H}{\partial v} \\
F_{Hv3} &\equiv \frac{\partial K_H}{\partial v} = -z_H \frac{\partial Y_H}{\partial v}
\end{aligned}
$$

These values can be calculated analytically. Consider the ship in forward motion under external disturbances using an autopilot. Then, $\Delta\delta$ is assumed to be expressed as follows:

$$
\begin{aligned}
\Delta\delta &= -G_1 \Delta\psi - G_2 \Delta r \\
&= [G]\{x\} \qquad (44)
\end{aligned}
$$

where $[G] = (0, -G_2, 0, -G_1, 0)$. G_1 and G_2 are called control gains. Then, the motion equation, Eq.(41) is rewritten as follows:

$$
\{\dot{x}\} = [A]^{-1}\left([B] + \{d\}[G]\right)\{x\} \qquad (45)
$$

Thus, the unsteady terms $\{x\}$ can be calculated by $[A]^{-1}([B] + \{d\}[G])$ as shown in Eq.(45). If the eigenvalues of the square matrix of 5×5 of $[A]^{-1}([B] + \{d\}[G])$ are obtained, it is easy to determine if the target ship is stable or not, for course keeping. The motion becomes stable if all the real parts of the eigenvalues are negative, and the motion becomes unstable even if one of them is positive.

4 Studied Ship

4.1 Principal particulars

A PCC was selected as the study ship in this study. Table 1 shows the principal particulars of the PCC. The load condition is full load even keel. In the table, L denotes the length between perpendiculars, B denotes the breadth, d denotes the draft, ∇ denotes the displacement volume, x_G denotes the longitudinal position of the center of gravity (fore position from the midship was positive), C_b denotes the block coefficient, $\overline{GM}$ denotes the metacentric height, $\overline{KM}$ denotes the metacenter height above baseline, D_P denotes the propeller diameter, $A_R/(Ld)$ denotes the rudder area ratio, H_R denotes the rudder span length, and A_X and A_Y denote the front and side profile areas of the ship in air, respectively. The radius of yaw gyration k_{zz} is assumed to be $0.25L$. Fig.2 shows the side profile of the PCC[2], and Fig.3 shows the body plan of the ship.

Table 1: Principal particulars of a PCC

items	value
L (m)	180.00
B (m)	32.20
d (m)	8.20
∇ (m^3)	26000
x_G (m)	-2.53
C_b	0.547
$\overline{GM}$ (m)	1.25
$\overline{KM}$ (m)	15.60
D_P (m)	6.00
$A_R/(Ld)$	1/39.5
H_R (m)	7.200
A_X (m^2)	859
A_Y (m^2)	4387

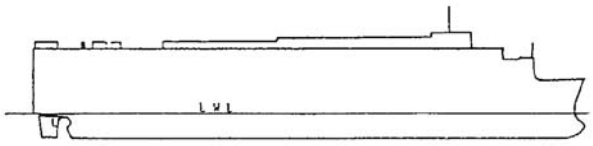

Fig. 2: Ship profile of the PCC

4.2 Main engine and propulsive performance

Two main engines are considered in this study to capture the effect of the difference between the engine outputs on the SSC and the CS for the PCC. Table 2 shows the specifications of the two main engines. As the base engine of the PCC, the engine power

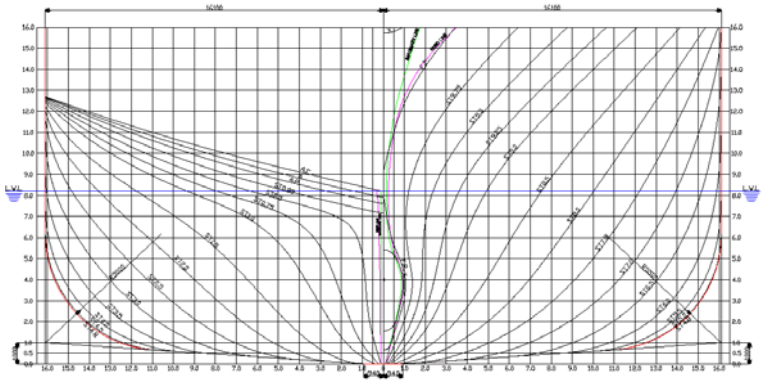

Fig. 3: Body plan of the PCC

at maximum continuous rating (P_{MCR}) was selected to be 13,000 kW, and the propeller revolution at MCR (N_{MCR}) was set as 105 rpm. The design speed (V_S) is 20 kn. This engine is called 'MCR13' in this study. On the other hand, energy efficiency is expected with smaller output energy. To investigate the effect of smaller engine output, a new engine of 9,820 kW is considered at MCR, which is mainly obtained to reduce the effective power (P_E) of the ship by 20%. This engine is called 'MCR10', in this study. The design speed for MCR10 (V_S) is 20 kn. Fig.4 shows the comparison of the effective power curves of MCR13 and MCR10.

In fact, it is very difficult to reduce the effective power/ship resistance by 20% without changing the ship hull form, but it simulates the following situations: specifically, it is considered to reduce the frictional resistance by using a special paint or micro air bubbles together with the reduction of the wave-making resistance by improving the bow shape. On the other hand, since the stern hull form is not changed, the hydrodynamic force coefficients on maneuvering and the self-propulsion factors are approximately the same in MCR13 and MCR10. In addition, it is assumed that the propellers have the same diameter for MCR13 and MCR10, and work near the optimum revolution for each. Then, since the propeller pitch ratio of the designed propeller for MCR10 was close to that for MCR13, the same propellers for MCR13 and MCR10 were used in the investigations.

Table 3 shows the coefficients representing the propeller thrust and torque (see Eqs.(17) and (18)). In the table, further, P_{NOR} is the engine power at Normal Rating (NOR), and N_{NOR} is the propeller revolution at NOR. Q_{EMAX} is the maximum torque for the main engines, and was obtained using the following formula: $Q_{EMAX} = P_{MCR}/(2\pi N_{MCR})$. It is important to note that MCR13 and MCR10 are virtual engines. Therefore, actual ships with these engines do not exist.

4.3 Hydrodynamic coefficients and parameters

The coefficients and parameters used for the calculations of the SSC and the CS are indicated in deep and shallow waters. The water depths are set as 38.5, 1.5 and 1.2 in h/d where h/d denotes the ratio of water depth (h) to ship draft (d). Conditions are classified as 'deep' when $h/d = 38.5$.

Table 2: Specification of main engines

symbol	MCR13	MCR10
P_{MCR} (kW)	13,000	9,820
N_{MCR} (rpm)	105	97
P_{NOR} (kW)	8,287	6,262
N_{NOR} (rpm)	92	86
Q_{EMAX} (ton-m)	120	100

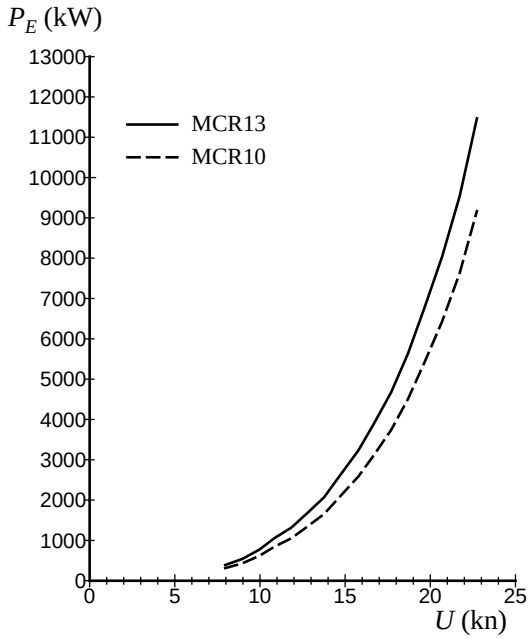

Fig. 4: Comparison of effective power curves in MCR10 and MCR13

4.3.1 Hydrodynamic derivatives excluding roll-coupling terms

Table 4 shows the hydrodynamic derivatives, coefficients, and parameters used in the calculations of the SSC and the CS under external disturbances. The derivatives and coefficients in the table were obtained by the captive model test in deep and shallow waters[30] using 3 m long ship model.

The flow straightening coefficient γ_R has asymmetrical characteristics and the different value is taken in port and starboard turning[17]. In this study, the average value of the γ_R in port and starboard turning, which is denoted by $\overline{\gamma_R}$, was used as shown in Table 4.

4.3.2 Roll-related hydrodynamic derivatives

The roll-related hydrodynamic derivatives were obtained by a circulation motion test with variations in the heel angles[33]. Table 5 shows the roll-related hydrodynamic derivatives that were used in the calculations.

Table 6 shows other parameters required for the calculations. z_H was obtained from the lateral force and roll moment measured by captive model test[33]. z_R was assumed

Table 3: Coefficients representing the propeller thrust and torque

symbol	value
k_0	0.4742
k_1	-0.2335
k_2	-0.0805
q_0	0.0721
q_1	-0.0288
q_2	-0.0113

Table 4: Hydrodynamic derivatives, coefficients and parameters

h/d	deep	1.5	1.2	h/d	deep	1.5	1.2
X'_{vv}	-0.0368	0.0460	0.3178	$m' + m'_x$	0.205	0.232	0.301
$X'_{vr} + m'_y$	0.140	0.493	0.663	$m' + m'_y$	0.331	0.413	0.544
X'_{rr}	0.0125	-0.0069	0.0038	$I'_{zz} + J'_{zz}$	0.0211	0.0262	0.0293
X'_{vvvv}	0.469	0.718	0.574	$1 - t_P$	0.850	0.773	0.695
Y'_v	-0.263	-0.993	-2.314	$1 - w_{P0}$	0.65	0.60	0.50
Y'_r	0.0381	0.0934	0.2089	η_R	1.02	1.02	1.02
Y'_{vvv}	-1.55	-5.03	-1.70	$1 - t_R$	0.792	0.738	0.776
Y'_{vvr}	-0.655	1.71	7.88	a_H	0.50	0.71	0.88
Y'_{vrr}	-0.738	-1.992	-3.042	x'_H	-0.467	-0.341	-0.322
Y'_{rrr}	-0.0566	-0.1246	-0.1542	ϵ	1.170	1.390	1.557
N'_v	-0.0977	-0.2043	-0.4620	κ	0.513	0.366	0.386
N'_r	-0.0505	-0.0689	-0.1286	$\overline{\gamma_R}$	0.615	0.695	0.530
N'_{vvv}	-0.173	-0.308	-0.914	l'_R	-0.811	-0.740	-0.917
N'_{vvr}	-0.627	-1.874	0.003				
N'_{vrr}	-0.0954	-0.0686	0.0880				
N'_{rrr}	-0.0353	-0.1495	-0.1469				

as the midpoint of the rudder span. The coefficients of the roll-extinction curve a and b, and radius of roll gyration k_{xx} in Table 6 were obtained by the roll decay test. Note that k_{xx} includes the added moment of inertia with respect to the roll.

4.4 External forces

Wind and waves are assumed to encounter the starboard side of the ship, so, the calculations were made only in the range where θ_W (or χ) is 0° to 180°. Aerodynamic force coefficients (C_{XA}, C_{YA}, C_{NA}, C_{KA}) of the ship were estimated by Fujiwara's method[34] and are shown in Fig.5.

Fig.6 shows the wave-induced steady force coefficients ($\overline{C_{XW}}$, $\overline{C_{YW}}$, $\overline{C_{NW}}$) at $F_n = 0$, and Fig.7 shows the wave-added resistance coefficient $\overline{C_{XW}}$ for different Froude numbers. The wave-induced steady forces in irregular waves were obtained by performing short-term predictions based on the wave-induced steady forces in regular waves, which were calculated by the zero-speed 3D panel method (3DPM) for the steady lateral force and

Table 5: Hydrodynamic derivatives related to heel angle ϕ

h/d	deep	1.5	1.2
$X'_{v\phi}$	0.0292	0.0046	-0.3804
$X'_{r\phi}$	0.0141	-0.0863	-0.0611
$X'_{\phi\phi}$	-0.0214	0.0647	0.1213
Y'_{ϕ}	0.0127	0.0444	0.1443
$Y'_{vv\phi}$	0.0433	2.966	4.699
$Y'_{v\phi\phi}$	0.1318	-3.749	-7.715
$Y'_{r\phi\phi}$	-0.3476	0.739	2.533
$Y_{rr\phi}$	0.1878	0.8969	2.264
N'_{ϕ}	-0.0109	-0.0591	-0.1080
$N'_{vv\phi}$	-0.3504	-0.8497	0.1825
$N'_{v\phi\phi}$	-0.1731	-0.6035	-1.947
$N'_{r\phi\phi}$	0.1277	0.4444	1.315
$N_{rr\phi}$	-0.0288	0.0189	0.2669

Table 6: Parameters related to roll motion

h/d	deep	1.5	1.2
z_H/d	0.285	-0.160	-0.292
z_R/d	0.57	0.57	0.57
a $(-)$	0.081	0.115	0.201
b $(1/^\circ)$	0.056	0.055	0.033
k_{xx}/B	0.31	0.31	0.32

the yaw moment, and the strip theory-based Kochin-function method (SKFM) for added resistance [32]. Then, the International Towing Tank Conference (ITTC) spectrum was used as the wave spectrum $S_{\zeta\zeta}(\omega)$, and the $\cos^2$-function was used as the wave direction distribution function $G(\theta)$.

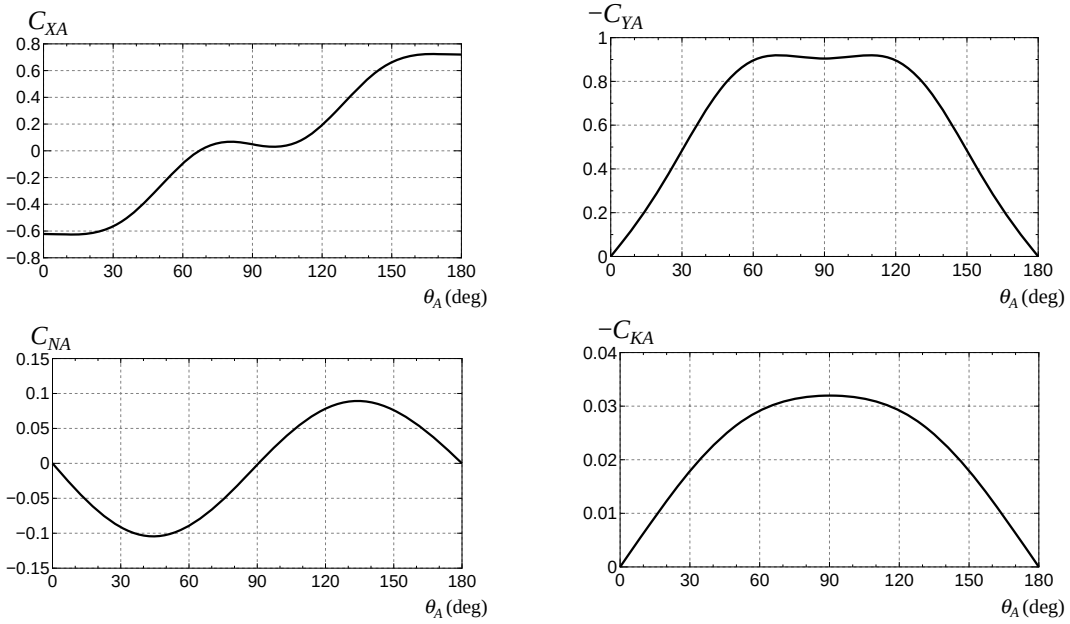

Fig. 5: Aerodynamic force coefficients

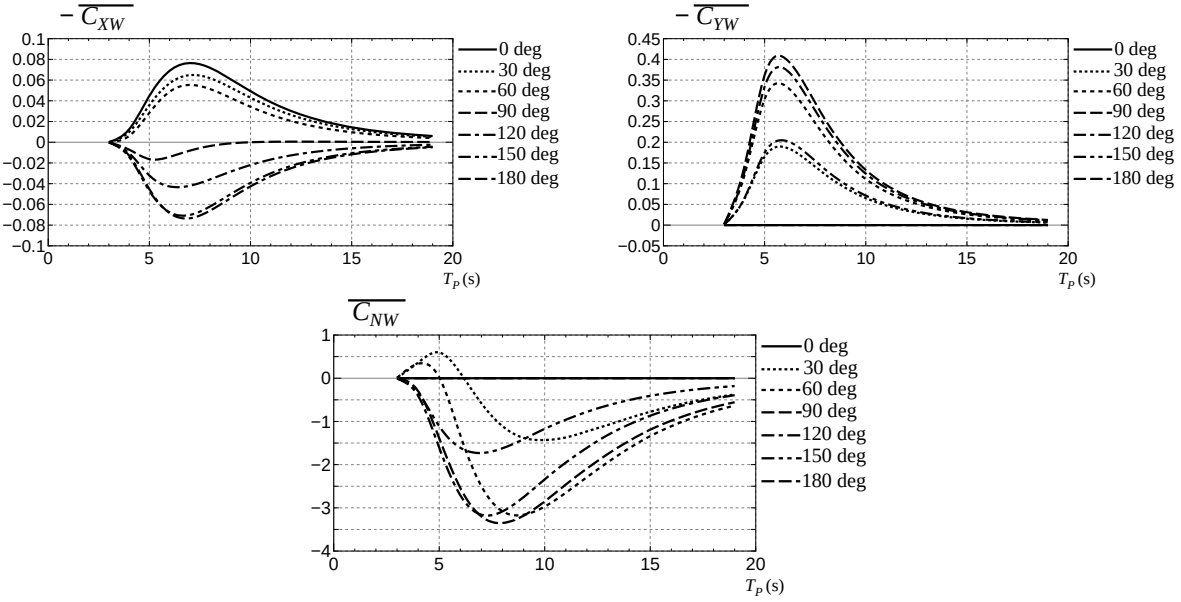

Fig. 6: Wave-induced steady force coefficients at $F_n = 0$

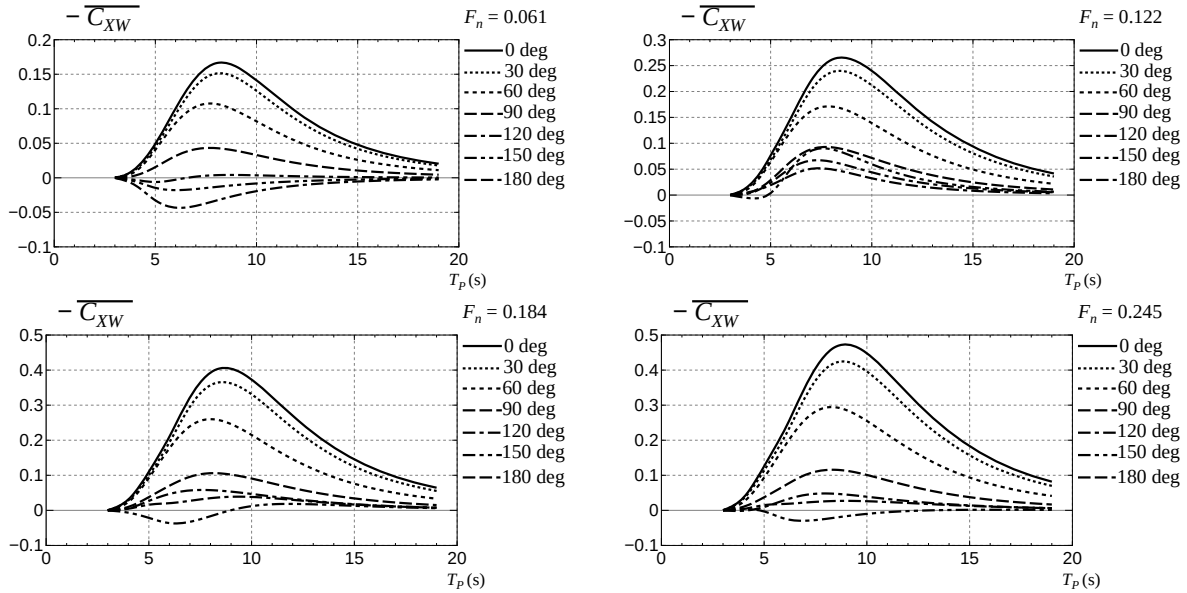

Fig. 7: Wave-added resistance coefficient $\overline{C_{XW}}$ for different Froude numbers

5 Maneuvering Limit of PCC in Deep Water

The SSC and the CS of the PCC moving in deep water is considered, maintaining the heading angle $\psi = 0°$ under steady external disturbances. Based on the SSC and the CS results, the maneuvering limit of the ship in adverse weather conditions is discussed. Here, the main engine is supposed to be used in the condition of 'Navigation-Full' (N-Full) with the propeller revolution N_{NOR}, where the ship sails at 20 kn in calm water.

5.1 External disturbance conditions

Table 7 shows the conditions of wind and waves in the predictions of the SSC and the CS. The conditions are classified by the Beaufort (BF) Scale, although the BF scale represents the strength of the wind speed originally. The wind speed by the BF scale is not defined by one value, but by a range of values. For instance, 10.8 m/s to 13.9 m/s for BF6. To ensure safe navigation, the highest wind speed was selected for each BF scale as the absolute wind velocity U_W in this study. The significant wave height $H_{1/3}$ was assumed for each BF scale as shown in Table 7, and the wave direction χ is also assumed to be the same as the absolute wind direction θ_W. Further, the average wave period T_P was varied, ranging from 6.0 s to 14.0 s with an interval of 1.0 s for the calculations.

Table 7: Conditions of wind and waves

Beaufort Scale	BF6	BF7	BF8	BF9	BF10
$H_{1/3}$ (m)	3	4	5.5	7	9
U_W (m/s)	13.9	17.2	20.8	24.5	28.5

5.2 Steady sailing condition

Fig.8 shows the comparison of the SSCs, including the longitudinal ship velocity component u_0, the check helm δ_0, the hull drift angle β_0 defined by ($\equiv \tan^{-1}(-v_0/u_0)$), and the heel angle ϕ_0 for MCR13 and MCR10 at $T_P = 10$s as calculation examples. The horizontal axis represents the absolute wind direction θ_W (wave direction χ is the same). u_0 drops significantly at the head waves (wind) direction with an increase of the BF scale. The speed drop in MCR10 is slightly larger than that in MCR13 due to the effect of smaller engine output. The absolute value of δ_0 reaches the maximum at about 100° in θ_W (χ), and the maximum value in MCR10 is slightly larger than that in MCR13. However, the maximum value is almost 10° in BF10 for both MCR10 and MCR13, and there is a safety margin for maximum rudder angle 35°. β_0 is over 15° in BF10 with the region of 15° to 60° of θ_W for both MCR10 and MCR13. The maximum value of β_0 in MCR10 is larger, at about 3° than that in MCR13. Thus, a larger check helm and larger drift angle are obtained in MCR10. It is considered that the small engine output in MCR10 leads to a low propeller load, thereby reducing the rudder force. ϕ_0 reaches the peak at around 90° which is the direction of the beam wind and waves, and the maximum absolute value is about 4° in BF10 for both MCR10 and MCR13. The magnitude is small, and no problem arises in the case of navigation safety.

Fig.9 shows calculation results of propeller torque in adverse weather conditions at $T_P = 10$s. In head wind and waves of BF10, the propeller torque is over the torque limit (Q_{EMAX}) for both MCR10 and MCR13, therefore, the torque rich phenomenon occurs. For MCR10, torque rich also occurs in BF9. In this case, the propeller revolution will be reduced to be within the torque limit.

It can be said that there is a sufficient margin for maximum rudder angle 35°, in the check helm for both MCR10 and MCR13. In the MCR10, the speed drop becomes larger and the absolute values of the check helm and the hull drift angle become larger compared to that in MCR13. Additionally, MCR10 may develop torque rich more easily than MCR13. Although there is a possibility of maneuverability becoming worse in adverse weather conditions in MCR10, it is not at an unsafe level.

5.3 Course stability

Next, the course stability is examined while changing the control gain (G_1, G_2) of the autopilot as a measure of the difficulty of maneuvering. The gains are changed as follows:

1. $(G_1, G_2) = (0,0)$
2. $(G_1, G_2) = (1,10\text{s})$
3. $(G_1, G_2) = (3,30\text{s})$

where 1. denotes no control, 2. denotes control with weak sensitivity, and 3. denotes normal control. The calculations for MCR13 are performed in this section.

Fig.10 shows the calculated results with respect to course stability in BF9 and BF10. In the figure, the radius from the origin denotes the average wave period (T_P), and the angle from the vertical axis indicates the wind (waves) direction (θ_W or χ). Direction of the upward vertical axis is 0°, direction of the downward vertical axis is 180° and that of the horizontal axis is 90°. In the graph, a circle denotes stability for course keeping and a blackening square denotes unstable conditions. The studied ship becomes unstable for course keeping in head and following wind (waves) directions when the control gains are zero, even though the ship is stable when sailing in calm water. The unstable area increases with an increase of the BF scale. In contrast, the ship becomes completely stable by applying the weak control with $(G_1, G_2) = (1,10\text{s})$. This tendency is similar to the investigated result of the course stability for a ship in wind[35][25]. Even if the ship is unstable in adverse weather conditions, the ship can be easily made stable for course keeping using autopilot. When employing a larger gain of $(G_1, G_2) = (3,30\text{s})$, the ship becomes even more stable. Therefore, it is considered that the studied ship has no problem in maintaining the course stability in adverse weather conditions.

5.4 Maneuvering limit

Based on the above discussions, the maneuvering limit of the ship in adverse weather conditions is considered. In order to discuss the maneuvering limit in detail, the following conditions are assumed, where the ship can sail safely while maintaining its course:

C1: Ship speed u_0 is more than 6 kn.

C2: Torque rich does not occur. (The propeller torque Q is less than 120 ton-m for MCR13, and less than 100 ton-m for MCR10)

C3: Absolute value of check helm δ_0 is less than 35°.

C4: Absolute value of hull drift angle β_0 is less than 30°.

C5: Absolute value of heel angle ϕ_0 is less than 5°.

C6: Ship is stable for course keeping. (The control gains for the autopilot are assumed to be $G_1 = 3$ and $G_2 = 30$s).

The minimum ship speed was assumed to be 6 kn in the worst case, on the assumption that the maximum current velocity is 2 kn and the necessary ship velocity is 4 kn.

If the conditions mentioned above are satisfied for all wind (waves) directions under a certain BF scale, it can be regarded that the ship can navigate safely in the BF scale. If not, it means that the BF scale is the limiting environmental condition for safe navigation. This condition is determined as the maneuvering limit.

Fig.11 shows the unsafe points of the ship in MCR10 and MCR13. In BF6 to BF10, the absolute value of δ_0 is always smaller than 35°, and β_0 and ϕ_0 also never exceed the limiting values assumed. In addition, the ship is always stable for course keeping in BF6 to BF10 as mentioned in sub-section 5.3, that is, the present ship always satisfies the conditions ranging from C3 to C6. Therefore, the only problems are the conditions of C1 (minimum speed is 6 kn), and C2 (occurrence of torque rich). In BF10 of MCR13, the unsafe points where the conditions of C1 and C2 are not satisfied, appear in the region of 0° to 30° for the wind (waves) direction (θ_W or χ), although the unsafe points disappear until BF9. However, in MCR10, unsafe points disappear until BF8. In BF9, the torque rich condition occurs in the range of 0° to 30° for θ_W (or χ). In BF10, the unsafe points where the conditions of C1 and C2 are not satisfied, appear in the region of 0° to 50° for θ_W (or χ). Further, in the region of 90° to 180° for θ_W (or χ), the unsafe points do not exist for both MCR10 and MCR13. From the results, it is demonstrated that the limiting environmental condition for the safe navigation (maneuvering limit) is BF9 in MCR13, and is BF8 in MCR10. For MCR10 to achieve the same level as the maneuvering limit of MCR13, it is desirable to make rudder force large[36].

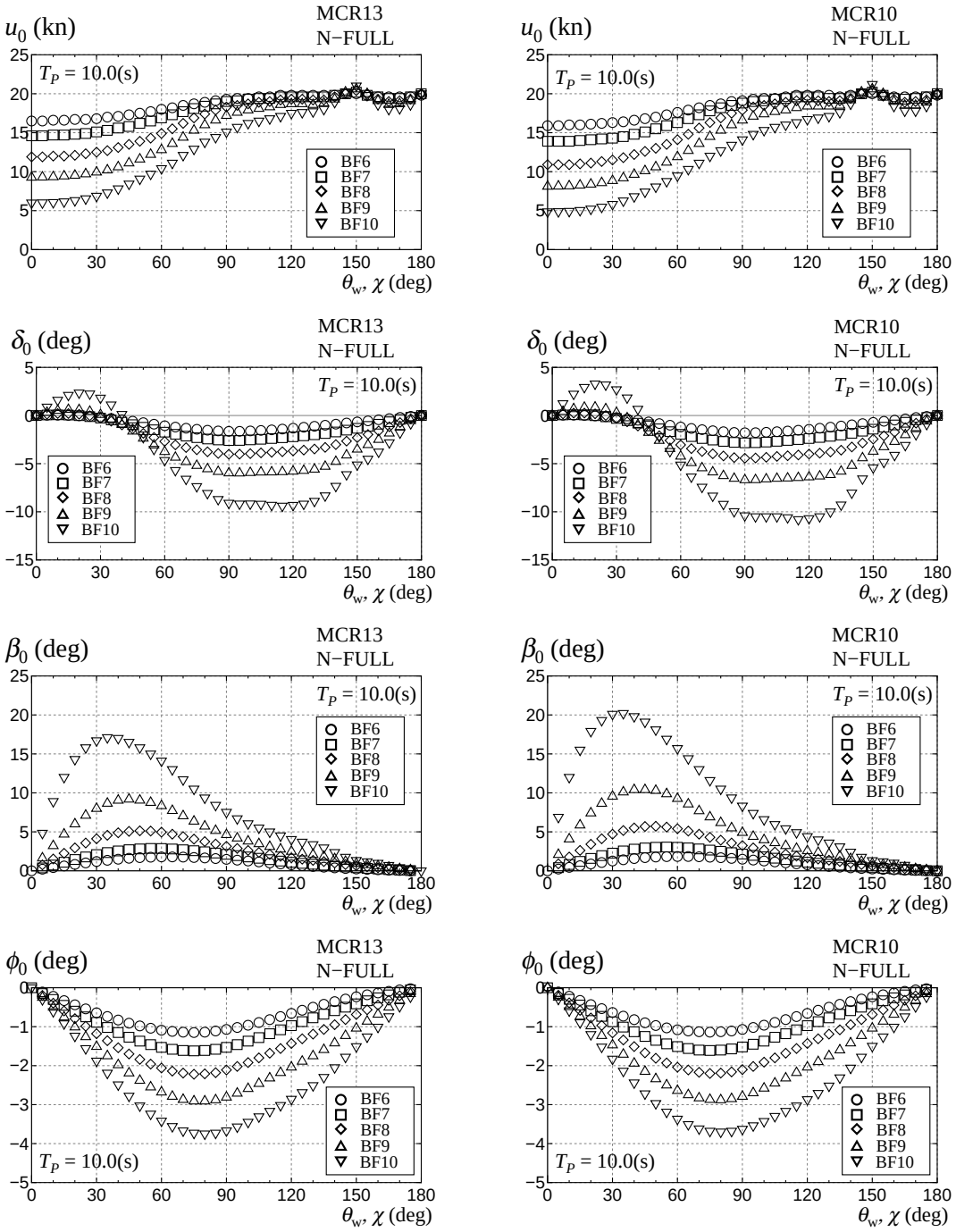

Fig. 8: Steady sailing conditions in adverse weather conditions at $T_P = 10$s (left: MCR13, right: MCR10)

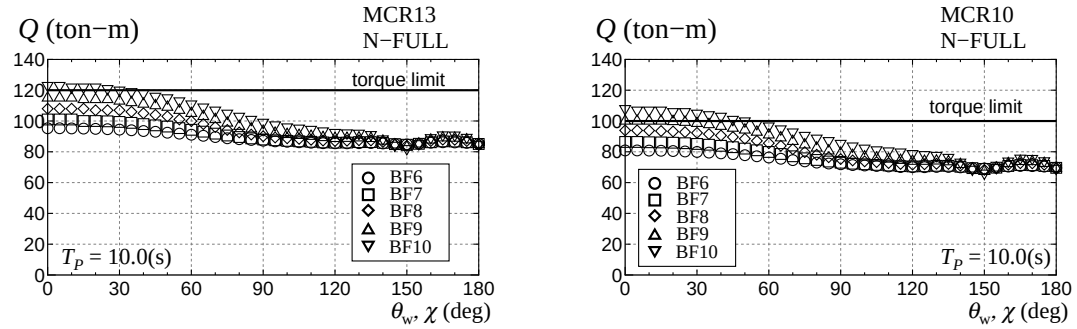

Fig. 9: Propeller torque in adverse weather conditions at $T_P = 10$s (left: MCR13, right: MCR10)

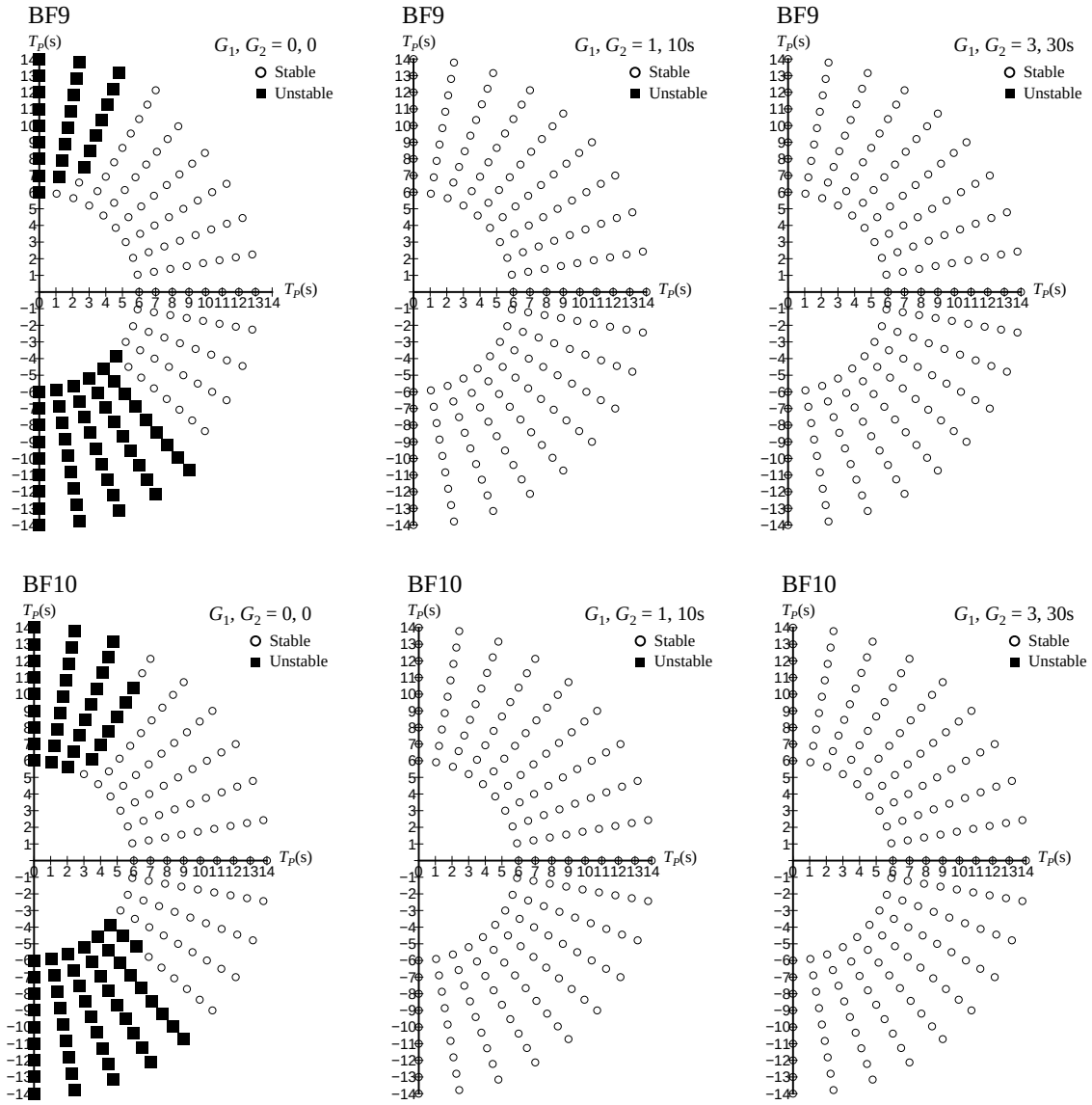

Fig. 10: Effect of control gain on course stability in BF9 and BF10 for MCR13

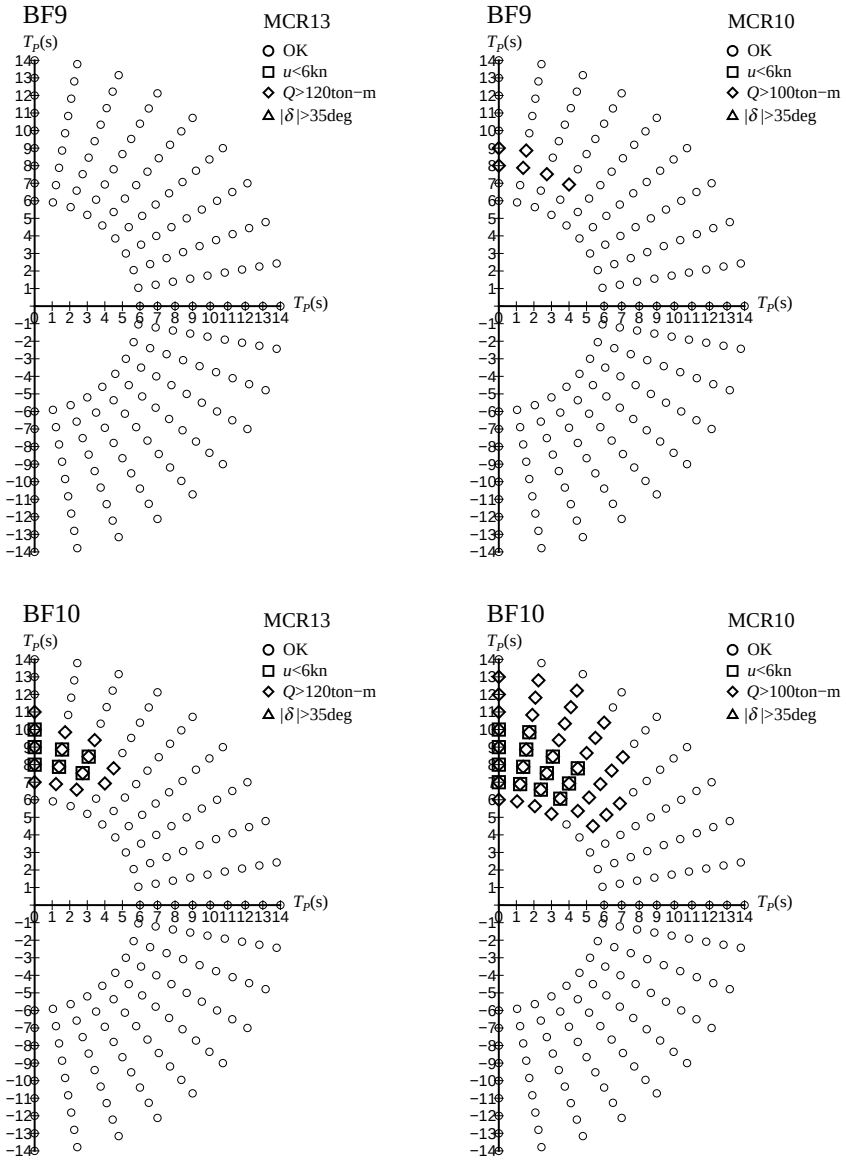

Fig. 11: Unsafe points in BF9 and BF10 (left: MCR13, right: MCR10)

6 Maneuvering Limit of PCC in Shallow Water

The SSC and the CS of a ship moving in shallow water is considered, maintaining the heading angle $\psi = 0°$ under steady wind. Based on the results of the SSC and the CS, the maneuvering limit of the ship in steady wind is discussed here. The ship is assumed to be navigating in the harbor area, therefore, the wave effect is neglected. Here, the main engine is supposed to be used in the condition of 'Half' with the propeller revolution $N_P = 44$ rpm where the ship sails at 10 kn in deep and calm water. The SSC and the CS under steady wind in three different water depths are calculated, such as deep ($h/d = \infty$), $h/d = 1.5$, and $h/d = 1.2$.

6.1 Wind conditions

Table 8 shows the wind conditions for the calculations. The strength of the wind is represented as BF scale.

Table 8: Wind conditions

Beaufort Scale	BF6	BF7	BF8	BF9
U_W (m/s)	13.9	17.2	20.8	24.5

6.2 Steady sailing condition

The SSC was calculated based on the longitudinal ship velocity component u_0, the check helm δ_0, the hull drift angle β_0, and the heel angle ϕ_0 for MCR13 and MCR10.

Fig.12 shows the calculation results of u_0. In the graph, horizontal axis represents the absolute wind direction θ_W. u_0 drops significantly in more shallow water depth in the head wind direction (0° to 30°). This is because the water resistance increases with decrease of the water depth. The speed drop in MCR10 is slightly larger than that in MCR13, and this behaviour is the same as mentioned in the sub-section 5.2.

Figs.13 and 14 show the calculation results of δ_0 and β_0, respectively. In case the absolute value of δ_0 is over 35°, no-solution is deemed to exist, that is, the check helm does not exist. For a larger BF scale, the absolute value of δ_0 becomes larger and is over 35° in several places, and this characteristic is significant in deep water. β_0 also becomes large in deep water. With decrease of the water depth, the absolute values of linear derivatives such as Y'_v and N'_r increase as shown in Table 4. The large derivatives suppress the progress of the maneuvering motion in wind, and, as a result, β_0 becomes smaller in shallow water. Since δ_0 is determined to balance with the hull hydrodynamic forces, it becomes smaller in shallow water. Generally, the absolute values of δ_0 and β_0 become larger for MCR10 in any water depths compared to MCR13, because the small engine output in MCR10 leads to a low propeller load, thereby reducing the rudder force.

Fig.15 shows the calculation results of ϕ_0. ϕ_0 reaches the peak value at almost $\theta_W = 90°$, which is the beam wind direction, the maximum absolute value is about 3°, and the magnitude is sufficiently small safe navigation. The magnitude of ϕ_0 is roughly the same, between MCR10 and MCR13.

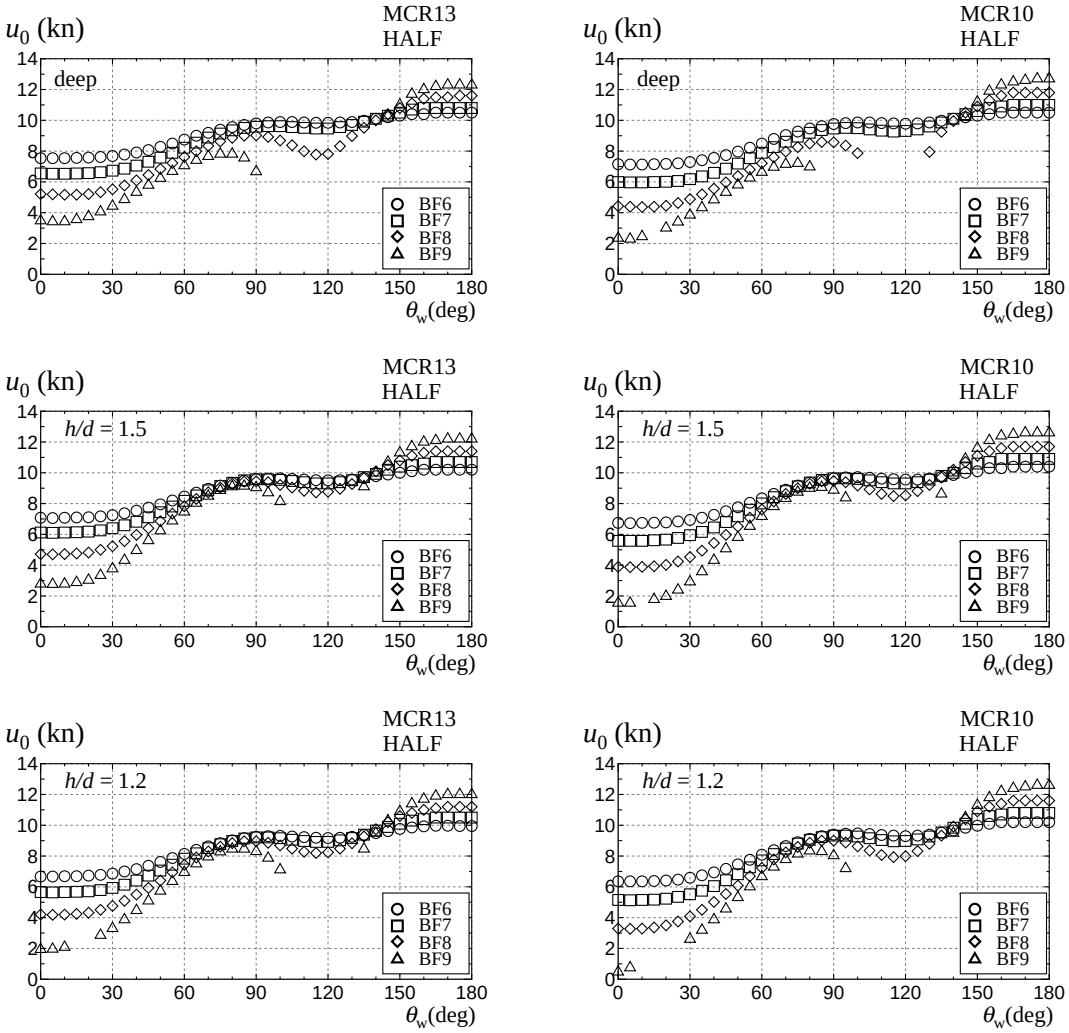

Fig. 12: Ship speed in three different water depths (left: MCR13, right: MCR10)

6.3 Course stability

In this section, the course stability is investigated while changing the control gain (G_1, G_2) of the autopilot as a measure of the difficulty of maneuvering. The gains are changed as follows:

1. $(G_1, G_2) = (0,0)$
2. $(G_1, G_2) = (1,10\text{s})$
3. $(G_1, G_2) = (3,30\text{s})$

The calculations were performed for MCR13.

Fig.16 shows the calculated results with respect to course stability in deep waters, $h/d = 1.5$ and $h/d = 1.2$. In the figure, the radius from the origin denotes the BF scale, and the angle from the vertical axis indicates the wind direction (θ_W), which are the same definitions as mentioned in sub-section 5.3. In the graph, a circle indicates stability for course keeping and a blackening square indicates unstable conditions. Further, a 'no

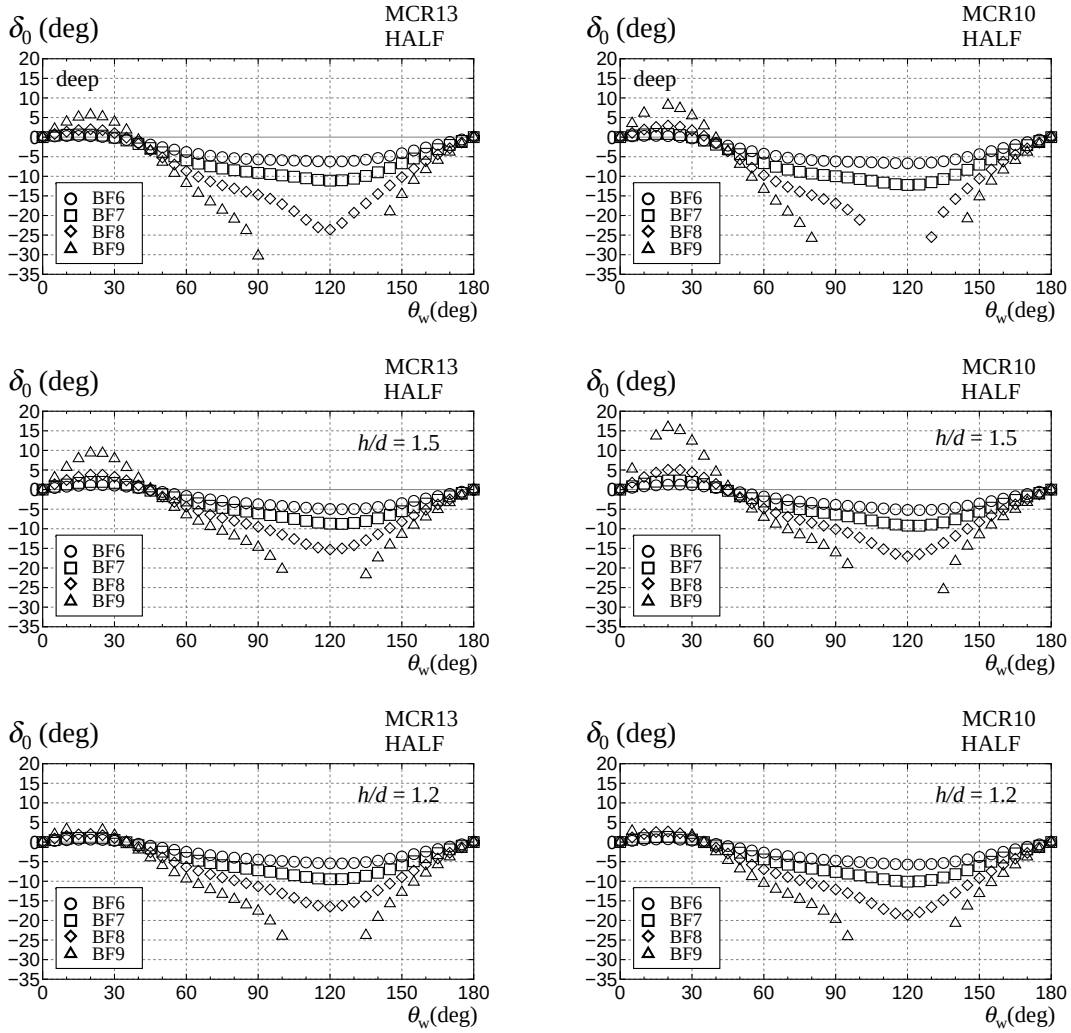

Fig. 13: Check helms in three different water depths (left: MCR13, right: MCR10)

solution' was marked in the graph, when the solution cannot be obtained numerically. 'No solution' usually occurs in quarter-following wind of 100° to 150° for θ_W. It is considered that the expected solution range is exceeded due to too much check helm (over 35°) in the calculation process.

The studied ship becomes unstable for course keeping in head and following wind directions when the control gains are zero, though the ship sailing in calm water is stable. Such behaviour is the same as the result mentioned in the sub-section 5.3 for the ship in deep water under adverse weather conditions. On the other hand, the ship becomes stable except for BF9 by applying the weak control with $(G_1, G_2) = (1,10s)$. When employing the larger gain of $(G_1, G_2) = (3,30s)$, the ship becomes completely stable. Even if the ship is unstable in such situation, the ship can be easily made stable using the autopilot. The studied ship has no problem in the course stability under steady wind in shallow water.

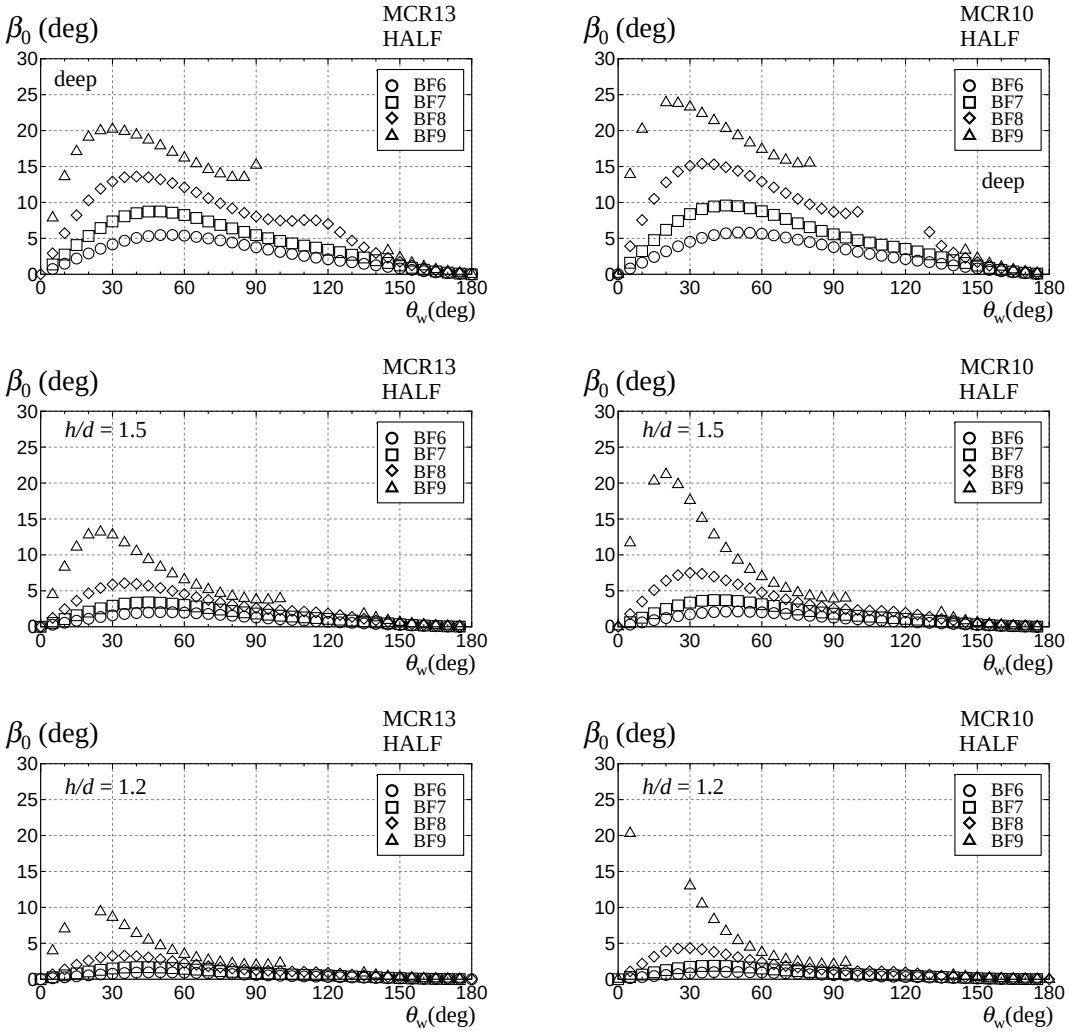

Fig. 14: Hull drift angles in three different water depths (left: MCR13, right: MCR10)

6.4 Maneuvering limit

Based on the above discussions, the maneuvering limit of the ship under steady wind is considered. In order to discuss the maneuvering limit in detail, the following conditions are assumed where the ship can sail safely while maintaining its course:

C1: Ship speed u_0 is more than 4 kn.

C2: Torque rich condition does not occur. (The propeller torque Q is less than 120 ton-m for MCR13, and less than 100 ton-m for MCR10)

C3: Absolute value of check helm δ_0 is less than 35°.

C4: Absolute value of hull drift angle β_0 is less than 30°.

C5: Absolute value of heel angle ϕ_0 is less than 5°.

C6: Ship is stable for course keeping. (The control gains for the autopilot (see Eq.(44)) are assumed to be $G_1 = 3$ and $G_2 = 30$s) which are the same as in section 5.

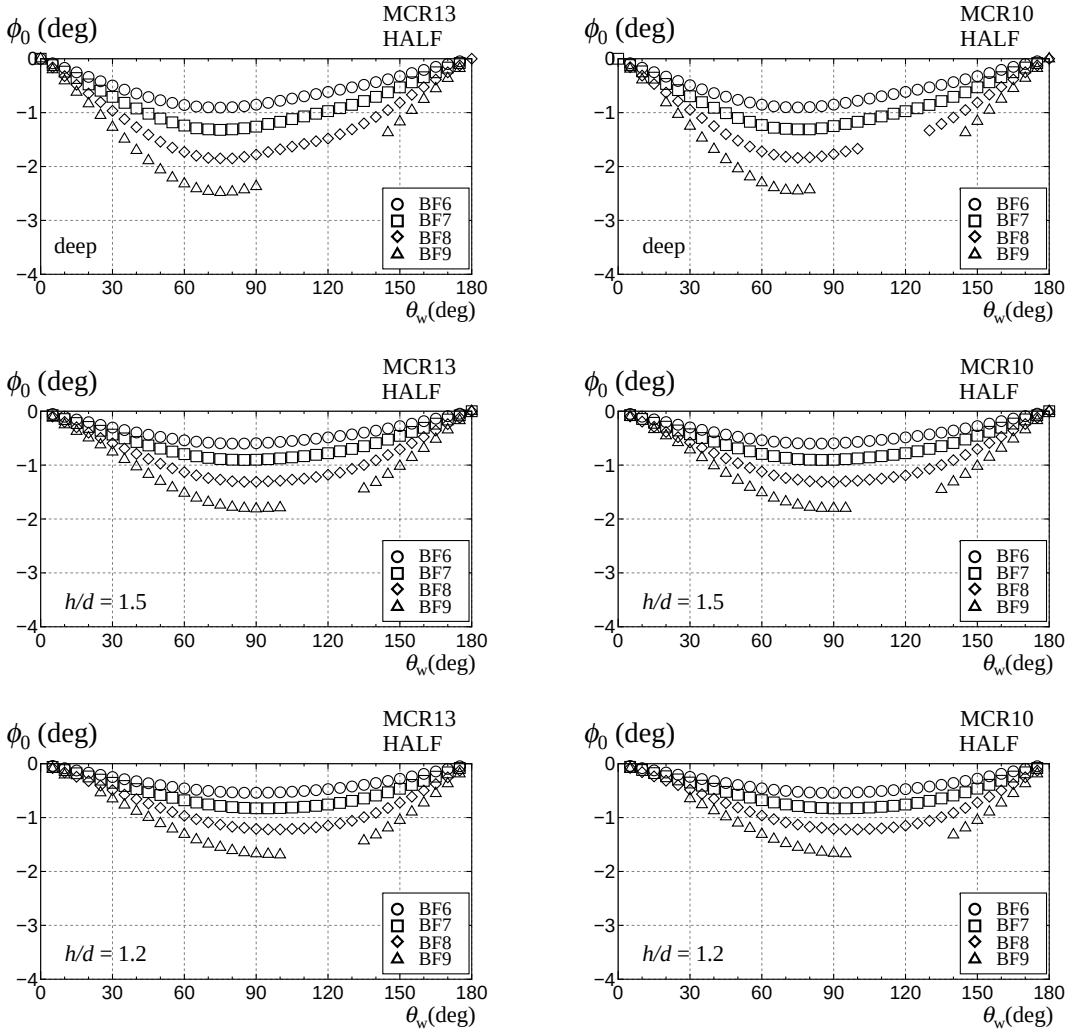

Fig. 15: Heel angles in three different water depths (left: MCR13, right: MCR10)

These conditions are the same as those mentioned in sub-section 5.4 except for the C1 condition about u_0.

Fig.17 shows the unsafe points of the ship in MCR10 and MCR13 in three different water depths. β_0 and ϕ_0 never exceed the assumed limiting values. The presented ship is always stable for course keeping in any water depth when autopilot is appropriately used as mentioned in sub-section 6.3. Torque rich condition never occurs because it is assumed that the main engine is operating at 'Half' capacity. The presented ship satisfies the conditions from C2, C4, C5, and C6. Therefore, the only problems are the conditions of C1 (minimum speed is 4 kn), and C3 (maximum rudder angle is 35°). In BF9 of MCR13, the unsafe points appear in the region of 0° to 40° for the wind direction (θ_W) because the C1 condition is not satisfied. In addition, the unsafe points where the absolute values of δ_0 exceed 35° (not satisfying C3) exist in the region of 100° to 140° for θ_W. For MCR10, the overall tendency is the same, however, the unsafe points increase for MCR10. The results show that the maneuvering limit becomes BF8 for MCR13 and BF7 for MCR10. The shallow water effect on the maneuvering limit is not so significant.

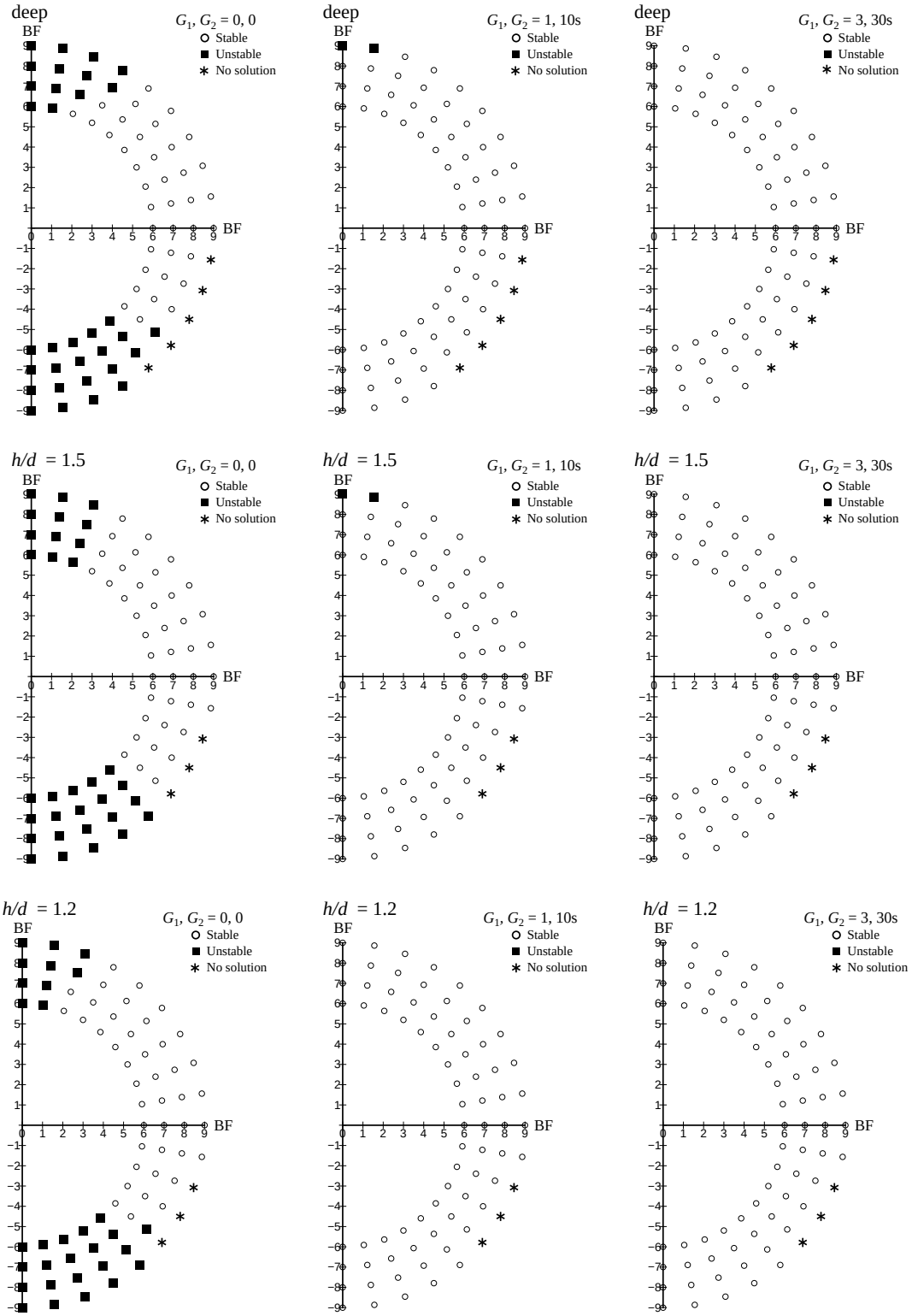

Fig. 16: Effect of control gain on course stability in three different water depths under steady wind

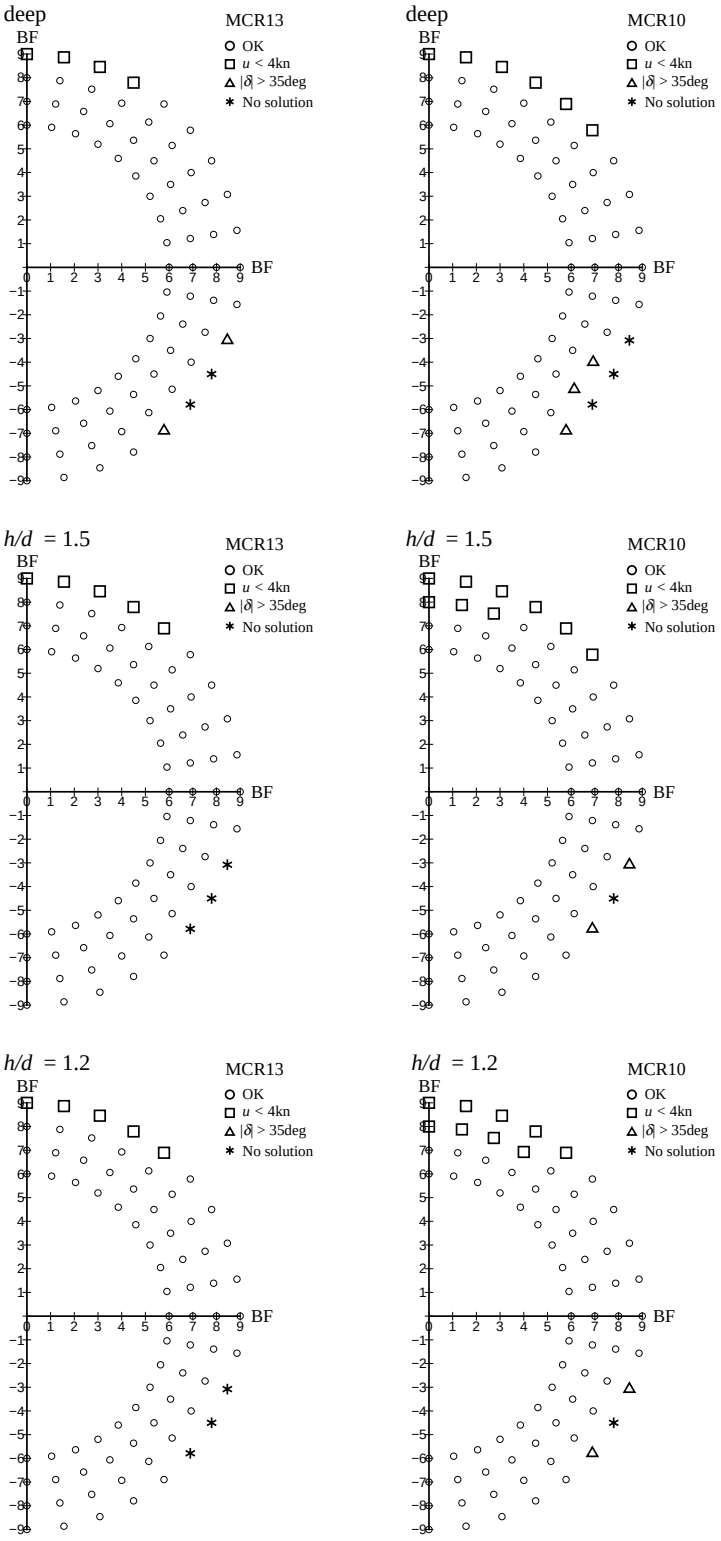

Fig. 17: Unsafe points in three different water depths (left: MCR13, right: MCR10)

7 Concluding Remarks

In this study, a method was proposed for analyzing the steady sailing condition (SSC) and the course stability (CS) of a ship under external disturbances due to wind and waves. The motion equations and the hydrodynamic force models are based on the MMG standard method[28], and the motion equation for roll[17] and wind forces and wave-induced steady forces as external disturbances[5] were added. Using the presented method, the SSC and the CS of a pure car carrier (PCC) with a ship length of 180 m subject to external disturbances was calculated in deep and shallow waters, and the limiting environmental condition for safe navigation (maneuvering limit) was discussed. In particular, the effect of the main engine output was investigated. As a result, the following conclusions were obtained:

- When the ship sails with a 'Navigation Full' engine output in deep water, the maneuvering limit, which is defined as the limiting environmental condition to enable the ship to keep the safe navigation, is Beaufort scale (BF) 9 in case of the standard engine output (MCR13). When the ship encounters a sea state higher than BF9, the ship cannot sail safely since the ship speed becomes lower than 6 kn, or the torque rich phenomenon occurs. In the case of a reduced engine output of approximately 30% (MCR10), the maneuvering limit is BF8. For a sea state higher than BF8, the ship cannot sail safely as the torque rich condition occurs when the wind (waves) direction is in the region of 0° to 30°. A significant effect due to reduced engine output on the maneuvering limit is observed. The course stability of the ship sailing under external disturbances is preserved when autopilot is used.

- When the ship sails with a 'Half' engine output in steady wind, the maneuvering limit is BF8 in any water depths for MCR13. For a sea state higher than BF8, the ship cannot sail safely since the ship speed becomes lower than 4 kn, in case the wind direction is 0° to 30° or the absolute value of the check helm exceeds 35°. For MCR10, the maneuvering limit is BF7 in any water depths. A significant effect on the maneuvering limit due to reduced engine output is observed, although the effect of the water depth is not so significant. There is no problem with the course stability of the ship sailing under external disturbances when autopilot is used.

Thus, the proposed method is useful in evaluating the SSC, the CS, and the maneuvering limit of the ship in deep and shallow waters under external disturbances.

The results with respect to the maneuvering limit of the PCC mentioned above were obtained under the conditions assumed in sub-sections 5.4 and 6.4 (base conditions), for the limiting values of ship speed, check helm, hull drift angle, heel angle and so on. In order to study the maneuvering limit extensively, the reliable base conditions have to be examined carefully, because the maneuvering limit depends on the base conditions. Further investigation on this is needed in future works.

Acknowledgements

This study was supported by JSPS KAKENHI Grant Number JP26249135. The authors express their sincere gratitude to Ms. A. Nishiyama for her assistance with the calculations of the SSC and the CS under external disturbances.

References

[1] Sezaki. Y. (1980): Effects of the Wind force to the Speed of a Car Carrier, J. Kansai Society of Naval Architects, Japan, No.179, pp.13-17 (in Japanese).

[2] Yoshimura, Y. and Nagashima, J. (1985): Estimation of the Manoeuvring Behavior of Ship in Uniform Wind, J. Society of Naval Architects of Japan, Vol.158, pp.125-136 (in Japanese).

[3] Hasegawa, K., Kang, D. H., Sano, M., Nagarajan, V. and Yamaguchi, M. (2006): A Study on Improving the Course-Keeping of a Pure Car Carrier in Windy Conditions, J. Marine Science and Technology, Vol.11, No.2, pp.76-87.

[4] Nagarajan, V., Kang, D. H., Hasegawa, K. and Nabeshima, K. (2008): Comparison of the Mariner Schilling Rudder and the Mariner Rudder for VLCCs in Strong Winds, J. Marine Science and Technology, Vol.13, No.1, pp.24-39.

[5] Yasukawa, H., Zaky, M., Yonemasu, I. and Miyake, R. (2017): Effect of Engine Output on Maneuverability of a VLCC in Still Water and Adverse Weather Conditions, J. Marine Science and Technology, Vol.22, No.3, pp.574-586.

[6] Eda, H. (1968): Low-Speed Controllability of Ships in Wind, J. Ship Research 12(3):63, pp.181-200.

[7] Ogawa, A. (1969): Calculation on the Steered Motion of a Ship under the action of External Forces(1), J. Society of Naval Architects of Japan, Vol.126, pp.107-120 (in Japanese).

[8] Ogawa, A., Koyama, T. and Kijima, K. (1977): MMG report-I, On the Mathematical Model of Ship Manoeuvring, Bulletin of Society of Naval Architects of Japan, No.575, pp.22-28 (in Japanese).

[9] Ishibashi, K. (1975): On Course Stability and Manoeuverable Range of Wind Velocity in the Uniform Wind, J. Society of Naval Architects of Japan, Vol.138, pp.165-177 (in Japanese).

[10] Tanaka, A., Yamagami, Y. Yamashita, Y. and Misumi, E. (1980): The Ship Manoevrbility in Strong Wind J. Kansai Society of Naval Architects, Japan, No.176, pp.1-10 (in Japanese).

[11] Martin, L. L. (1980): Ship Maneuvering and Control in Wind, SNAME Trans., Vol.88, pp.257-281.

[12] Hirano, M., Takashina, J. and Moriya, S. (1984): Ship Maneuverability in Wind, J. Society of Naval Architects of Japan, Vol.155, pp.122-131 (in Japanese).

[13] Eda, H. (1980): Rolling and Steering Performance of High Speed Ships, Proc. 13th Symp. on Naval Hydrodynamics, Tokyo, pp.427-439.

[14] Hirano, M. and Takashina, J. (1980): A Calculation of Ship Turning Motion Taking Coupling Effect due to Heel into Consideration, Trans. West-Japan Society of Naval Architects, No.59, pp.71-81.

[15] Son, K. and Nomoto, K. (1981): On the Coupled Motion of Steering and Rolling of a High Speed Container Ship, J. Society of Naval Architects of Japan, Vol.150, pp.232-244 (in Japanese).

[16] Yasukawa, H. and Yoshimura, Y. (2014): Roll-Coupling Effect on Ship Maneuverability, Ship Technology Research, Vol. 61, No.1, pp.16-32.

[17] Yasukawa, H., Sakuno, R. and Yoshimura, Y.(2019): Practical Maneuvering Simulation Method of Ships Considering the Roll-Coupling Effect, J. Marine Science and Technology, in press.

[18] Kadomatsu, K., Inoue, Y. and Takarada, N. (1990): On the Required Minimum Output of Main Propulsion Engine for Large Fat Ship with Considering Manoeuverability in Rough Seas, J. Society of Naval Architects of Japan, Vol.168, pp.171-182 (in Japanese).

[19] Spyrou, K. (1995): Yaw Stability of Ships in Steady Wind, Ship Technology Research, Vol.42, pp.21-30.

[20] Naito, S. and Takagishi, K. (1998): Time Mean Behavior of Large Full Ships in the Sea, J. Kansai Society of Naval Architects, Japan, No.229, pp.57-68 (in Japanese).

[21] Fujiwara, T., Ueno, M. and Ikeda, Y. (2005): Cruising Performance of Ships with Large Superstructures in Heavy Sea –1st report: Added resistance induced by wind–, J. Japan Society of Naval Architects and Ocean Engineers, Vol.2, pp.257-269 (in Japanese).

[22] Fujiwara, T., Ueno, M. and Ikeda, Y. (2006): Cruising Performance of Ships with Large Superstructures in Heavy Sea –2nd report: Added resistance induced by wind and waves, and optimum ship routing–, J. Japan Society of Naval Architects and Ocean Engineers, Vol.3, pp.147-155 (in Japanese).

[23] Umeda, N., Kawaida, D., Ooiwa, S., Matsuda, A. and Terada, D. (2016): Tank Test Results and Simulations in Adverse Weather Conditions, Symp. Minimum Engine Power Requirement of Ships, Japan Institute of Navigation, Japan Society of Naval Architects and Ocean Engineers, Tokyo, pp.51-56 (in Japanese).

[24] Asai, S. (1981): A Study on Check Helms for Course Keeping of a Ship under Steady External Forces, J. Society of Naval Architects of Japan, Vol.150, pp.245-253.

[25] Yasukawa, H., Hirono, T., Nakayama, Y. and Koh, K. K. (2012): Course Stability and Yaw Motion of a Ship in Steady Wind, J. Marine Science and Technology, Vol.17, No.3, pp.291-304.

[26] Yoshimura, Y. (1988): Mathematical Model for Manoeuvring Ship Motion in Shallow Water (2nd Report), – Mathematical Model at Slow Forward Speed –, J. Kansai Society of Naval Architects, Japan, No.210, pp.77-84 (in Japanese).

[27] Yoshimura, Y., Nakao, I. and Ishibashi, A. (2009): Unified Mathematical Model for Ocean and Harbour Manoeuvring, Proc. MARSIM2009, pp.M116-M124.

[28] Yasukawa, H. and Yoshimura, Y. (2015): Introduction of MMG Standard Method for Ship Maneuvering Predictions, J. Marine Science and Technology, Vol.20, No.1, pp.37-52.

[29] Hamamoto, M. and Kim, Y. (1993): A New Coordinate System and the Equations Describing Manoeuvring Motion of a Ship in Waves, J. Society of Naval Architects of Japan, Vol.173, pp.209-220 (in Japanese).

[30] Yoshimura, Y. (1984): Mathematical Model for the Manoeuvring Ship Motion in Shallow Water, J. Kansai Society of Naval Architects, Japan, No.200, pp.41-51 (in Japanese).

[31] Yasukawa, H., Zaky, M., Yamazaki, Y. and Amii, H. (2017): Maneuverability of C_b-Series Full Hull Ships (2nd report: maneuvering simulations) J. Japan Society of Naval Architects and Ocean Engineers, No.26, pp.63-70 (in Japanese).

[32] Yasukawa, H., Hirata, N., Matsumoto, A., Kuroiwa and Mizokami, S. (2019): Evaluations of Wave-Induced Steady Forces and Turning Motion of a Full Hull Ship in Waves, J. Marine Science and Technology, Vol.24, No.1, pp.1-15.

[33] Yasukawa, H. (2019): Maneuvering Hydrodynamic Derivatives and Course Stability of a Ship Close to Bank, Proc. 5th International Conference on Ship Manoeuvring in Shallow and Confined Water: Manoeuvring in Waves, Wind, Current, Ostend, Belgium (to be presented).

[34] Fujiwara, T., Ueno, M., and Nimura, T. (1998): Estimation of Wind Forces and Moments Acting on Ships, J. Society of Naval Architects of Japan, No.183, pp.77-90. (in Japanese).

[35] Spyrou, K. J., Tigkas, I. and Chatzis, A. (2007): Dynamics of a Ship Steering in Wind Revisited, Journal of Ship Research, Vol.51, No.2, pp.160-173.

[36] Zaky, M., Sano, M. and Yasukawa, H. (2019): Improvement of Maneuverability in a VLCC by a high lift rudder, Ocean Engineering (in press).